Altered expression levels of long non-coding natural antisense transcripts overlapping the UGT73C6 gene affect rosette size in Arabidopsis thaliana

Shiv Kumar Meena, Michel Heidecker, Susanne Engelmann, Ammar Jaber, Tebbe de Vries, Saskia Triller, Katja Baumann-kaschig, Steffen Abel, Sven-erik Behrens, Selma Gago-zachert

▶ **To cite this version:**

Shiv Kumar Meena, Michel Heidecker, Susanne Engelmann, Ammar Jaber, Tebbe de Vries, et al.. Altered expression levels of long non-coding natural antisense transcripts overlapping the UGT73C6 gene affect rosette size in Arabidopsis thaliana. The Plant Journal, 2022, 113 (3), pp.460 - 477. 10.1111/tpj.16058 . hal-04059666

HAL Id: hal-04059666
https://hal.science/hal-04059666v1

Submitted on 5 Apr 2023

HAL is a multi-disciplinary open access archive for the deposit and dissemination of scientific research documents, whether they are published or not. The documents may come from teaching and research institutions in France or abroad, or from public or private research centers.

L'archive ouverte pluridisciplinaire **HAL**, est destinée au dépôt et à la diffusion de documents scientifiques de niveau recherche, publiés ou non, émanant des établissements d'enseignement et de recherche français ou étrangers, des laboratoires publics ou privés.

the plant journal

SEB SOCIETY FOR EXPERIMENTAL BIOLOGY

The Plant Journal (2023) **113,** 460–477 doi: 10.1111/tpj.16058

Altered expression levels of long non-coding natural antisense transcripts overlapping the *UGT73C6* gene affect rosette size in *Arabidopsis thaliana*

Shiv Kumar Meena[1,†], Michel Heidecker[1,‡], Susanne Engelmann[1], Ammar Jaber[1], Tebbe de Vries[1,§], Saskia Triller[1,¶], Katja Baumann-Kaschig[1], Steffen Abel[1], Sven-Erik Behrens[2] and Selma Gago-Zachert[1,2,*]

[1]*Department of Molecular Signal Processing, Leibniz Institute of Plant Biochemistry, Halle/Saale D-06120, Germany,*
[2]*Section Microbial Biotechnology, Institute of Biochemistry and Biotechnology, Martin Luther University Halle-Wittenberg, Halle/Saale D-06120, Germany*

Received 3 December 2021; accepted 29 November 2022; published online 10 December 2022.
*For correspondence (e-mail selma.gago-zachert@bct.uni-halle.de).
[†]Present address: Department of Forest Genetics and Plant Physiology, Umeå Plant Science Centre, Swedish University of Agricultural Sciences, 90187, Umeå, Sweden
[‡]Present address: Department of Developmental Genomics and Genetics, Institute of Plant Sciences Paris-Saclay (IPS2), Université de Paris, Bat 630, 91192, Gif sur Yvette, France
[§]Present address: Department of Biology, ETH Zurich, Zurich, 8093, Switzerland
[¶]Present address: Fraunhofer Institute for Molecular Biology and Applied Ecology (IME), Forckenbeckstraße 6, 52074, Aachen, Germany

SUMMARY

Natural antisense long non-coding RNAs (lncNATs) are involved in the regulation of gene expression in plants, modulating different relevant developmental processes and responses to various stimuli. We have identified and characterized two lncNATs (*NAT1*$_{UGT73C6}$ and *NAT2*$_{UGT73C6}$, collectively *NATs*$_{UGT73C6}$) from *Arabidopsis thaliana* that are transcribed from a gene fully overlapping *UGT73C6*, a member of the *UGT73C* subfamily of genes encoding UDP-glycosyltransferases (UGTs). Expression of both *NATs*$_{UGT73C6}$ is developmentally controlled and occurs independently of the transcription of *UGT73C6* in *cis*. Downregulation of *NATs*$_{UGT73C6}$ levels through artificial microRNAs results in a reduction of the rosette area, while constitutive overexpression of *NAT1*$_{UGT73C6}$ or *NAT2*$_{UGT73C6}$ leads to the opposite phenotype, an increase in rosette size. This activity of *NATs*$_{UGT73C6}$ relies on its RNA sequence and, although modulation of *UGT73C6* in *cis* cannot be excluded, the observed phenotypes are not a consequence of the regulation of *UGT73C6* in *trans*. The *NATs*$_{UGT73C6}$ levels were shown to affect cell proliferation and thus individual leaf size. Consistent with this concept, our data suggest that the *NATs*$_{UGT73C6}$ influence the expression levels of key transcription factors involved in regulating leaf growth by modulating cell proliferation. These findings thus reveal an additional regulatory layer on the process of leaf growth. In this work, we characterized at the molecular level two long non-coding RNAs (*NATs*$_{UGT73C6}$) that are transcribed in the opposite direction to *UGT73C6*, a gene encoding a glucosyltransferase involved in brassinosteroid homeostasis in *A. thaliana*. Our results indicate that *NATs*$_{UGT73C6}$ expression influences leaf growth by acting in *trans* and by modulating the levels of transcription factors that are involved in the regulation of cell proliferation.

Keywords: *Arabidopsis thaliana*, natural antisense transcripts, long non-coding RNAs, leaf development, gene expression regulation, transcription factors.

INTRODUCTION

Long non-coding RNAs (lncRNAs) are transcripts of more than 200 nucleotides without protein-coding capacity (Mercer et al., 2009). Many lncRNAs have been shown to be important regulators of gene expression (Rinn & Chang, 2012). lncRNAs exert their activity in diverse cellular contexts, and participate in different biological processes regulating chromatin organization and transcription, mRNA stability and translation. Based on their relative location to nearby protein-coding genes, lncRNAs are classified as long non-coding natural antisense transcripts (lncNATs), and intronic, intergenic or promoter lncRNAs (Ariel et al., 2015; Rinn & Chang, 2012). lncNATs are transcripts generated from the DNA strand opposite to a

© 2022 The Authors.
The Plant Journal published by Society for Experimental Biology and John Wiley & Sons Ltd.
This is an open access article under the terms of the Creative Commons Attribution-NonCommercial-NoDerivs License, which permits use and distribution in any medium, provided the original work is properly cited, the use is non-commercial and no modifications or adaptations are made.

protein-coding gene and overlap at least one coding exon (Ariel et al., 2015). Natural antisense transcripts (NATs) are distinguished into *cis*- and *trans*-NATs. In the case of *cis*-NATs, sense and antisense transcripts are generated from the same genomic locus and show perfect complementarity, while *trans*-NATs are transcribed from a different locus and might share only partial sequence complementarity with the sense transcript (Lapidot & Pilpel, 2006). The mode of action of lncNATs to regulate their targets is diverse. In plants, it was initially proposed that endogenous small interfering RNAs (nat-siRNAs) generated by RNAi from sense-antisense RNA hybrids produced in response to certain environmental or developmental stimuli could regulate gene expression at the post-transcriptional level (Borsani et al., 2005; Zhang et al., 2013). Furthermore, it was proposed that lncNATs may act in *trans*, particularly when they are co-expressed and share high levels of sequence similarity with their potential targets (Wang et al., 2006). However, mounting evidence based on work published in recent years indicates that most nat-siRNAs are not associated with changes in the levels of both the sense and antisense transcripts, and may play only a minor role (Reis & Poirier, 2021). lncNATs were further shown to regulate gene expression through transcriptional collision, DNA methylation, histone modification, alteration of mRNA stability, and by modulation of mRNAs splicing, editing and translation (Lin et al., 2015).

The lncRNAs have been largely studied in mammalian, and particularly in human, cells. Less is known about their function in plants, where only a few lncNATs have been functionally characterized (Wang & Chekanova, 2017; Wu et al., 2020). These lncNATs are important regulators of gene expression, and are involved in the modulation of developmental processes and in the responses to different stimuli (Yu et al., 2019). In the model plant *Arabidopsis thaliana*, lncNATs are part of the control circuits of fundamental processes including germination (Fedak et al., 2016), flowering (Csorba et al., 2014; Henriques et al., 2017; Rosa et al., 2016; Zhao et al., 2018) and gametophyte development (Wunderlich et al., 2014). Furthermore, it has been reported that an antisense lncRNA is involved in cold acclimation (Kindgren et al., 2018). In rice, lncNATs modulate responses to phosphate starvation (Jabnoune et al., 2013), and are involved in the maintenance of leaf blade flattening (Liu et al., 2018). In tomato, a particular lncNAT, when overexpressed, was shown to confer resistance to the oomycete *Phytophthora infestans* (Cui et al., 2017).

Plant uridine diphosphate (UDP) glycosyl transferases (UGTs) are enzymes that transfer UDP-activated sugars to a variety of aglycone substrates, including hormones, secondary metabolites and xenobiotics (Ross et al., 2001). Glycosylation leads to changes in the target properties that alter their bioactivity and solubility, and plays an important role in maintaining cellular homeostasis by regulating the activity and location of important cellular metabolites and hormones. In *A. thaliana*, the UGT family contains 107 putative genes and 10 pseudogenes (Caputi et al., 2012; Ross et al., 2001). The *UGT73C* subfamily consists of seven genes, of which six, *UGT73C1*–*UGT73C6*, are clustered in a tandem repeat on chromosome 2 and exhibit high nucleotide identity (between 77% and 91%). A combination of *in vitro* and *in vivo* studies showed that UGT73C6 can glycosylate flavonoids (Ross et al., 2001). In addition, UGT73C5 and UGT73C6 were indicated to catalyze the *in vivo* 23-*O*-glycosylation of brassinosteroids (BRs; Husar et al., 2011; Poppenberger et al., 2005), i.e. plant steroid hormones that promote growth by modulating cell division, elongation and differentiation. Glycosylation leads to inactivation of the hormone and is therefore important, together with hydroxylation, for maintaining cellular homeostasis. Overexpression of *UGT73C6* or *UGT73C5* in *A. thaliana* accordingly results in phenotypes indicative of BR deficiency, with plants showing cabbage-like morphology and dark green leaves with short petioles. In addition, and correlated with the strength of overexpression, delayed flowering and senescence, and reduced fertility were observed (Husar et al., 2011; Poppenberger et al., 2005).

Leaf size and shape are determinants of the ability of plants to absorb sunlight and convert it into chemical energy through photosynthesis (Gonzalez et al., 2012). Leaf growth is a dynamic process regulated by two key, highly interrelated processes, namely cell division and cell expansion (Kalve et al., 2014). In Arabidopsis, founder cells located at the sides of the shoot apical meristem initiate leaf development (Vercruysse et al., 2020). After the initial phase of extensive cell proliferation throughout the leaf primordium, cell division ceases and further growth is supported mainly by cell expansion (Gonzalez et al., 2012). The latter process initiates at the leaf tip and follows a basipetal direction (Andriankaja et al., 2012). The precise regulation of cell proliferation and expansion mechanisms is therefore critical for determining final leaf size. Six gene modules are involved in the regulation of Arabidopsis leaf growth and one of them, the *GROWTH REGULATORY FACTOR* (*GRF*)-*GRF-INTERACTING FACTOR* (*GIF*) module, plays an important role in determining the cell number in leaves by controlling cell proliferation (Vercruysse et al., 2020).

In the present work, we show that alterations in the transcript levels of two *UGT73C6*-overlapping lncNATs ($NATs_{UGT73C6}$) lead to changes in rosette size of *A. thaliana*. Microscopic analyses indicate that these differences are mainly due to changes in cell number, suggesting that $NATs_{UGT73C6}$ levels affect cell proliferation. These phenotypic effects were shown to be due to $NATs_{UGT73C6}$ acting as *bona fide* non-coding RNAs. Our data suggest that $NATs_{UGT73C6}$ exert their function in *trans* and independently of the sense gene in a mechanism that excludes

© 2022 The Authors.

1365313x, 2023, 3, Downloaded from https://onlinelibrary.wiley.com/doi/10.1111/tpj.16058 by Universite Paris-Saclay, Wiley Online Library on [05/04/2023]. See the Terms and Conditions (https://onlinelibrary.wiley.com/terms-and-conditions) on Wiley Online Library for rules of use; OA articles are governed by the applicable Creative Commons License

downregulation of the *UGT73C* subfamily members but involves changes in the expression of important transcription factors from the *GRF-GIF* module.

RESULTS

NAT1$_{UGT73C6}$ and *NAT2*$_{UGT73C6}$, two lncRNAs overlapping the *UGT73C6* gene, are expressed in diverse organs and at different developmental stages of *Arabidopsis thaliana*

Analyzing the transcripts reported in the TAIR10 database, we identified two natural antisense transcripts (*At2g36792.1* and *At2g36792.2*) that overlap the *UGT73C6* gene. *In silico* analysis of the protein-coding capacity of both transcripts, hereafter referred to as *NAT1*$_{UGT73C6}$ and *NAT2*$_{UGT73C6}$ (for *At2g36792.1* and *At2g36792.2*, respectively) and collectively *NATs*$_{UGT73C6}$, revealed the presence of several open reading frames (ORFs) potentially encoding peptides of at least five amino acids. Most of the predicted peptides were smaller than 30 amino acids in length and none of them showed similarity to peptides present in the databases, nor did they have functional domains as determined using Pfam and PROSITE. Together, these data suggest that the transcripts are *bona fide* lncNATs.

To analyze the expression pattern of the individual *NATs*$_{UGT73C6}$, we generated transgenic lines in which the *uidA* gene (*GUS*), encoding β-glucoronidase (GUS), was placed under the control of 2054- and 2580-bp sequences upstream of the annotated transcription starts of *NAT1-UGT73C6* and *NAT2UGT73C6*, respectively, which were expected to contain the respective NATs promoters (Figure 1a). Analysis of *GUS* expression in several independent homozygous lines (three for *NAT1*$_{UGT73C6}$*:GUS* and five for *NAT2*$_{UGT73C6}$*:GUS*) revealed that both promoters were active and, interestingly, these activities were independent of the presence of the sense gene at the same locus. The selected promoters showed a distinct pattern of expression: the *NAT1*$_{UGT73C6}$ promoter was active exclusively in roots, whereas the activity of the *NAT2*$_{UGT73C6}$ promoter was detected only in the aerial organs, particularly in young leaves (Figure 1b). As the selected sequences overlap completely except for 526 bp at the 3′-end (Figure 1a), these results suggest that motifs present in the latter region are responsible for the expression of the *NAT2*$_{UGT73C6}$ promoter in aerial tissues and exclusion from expression in root tissue. Subsequent time course experiments confirmed that the promoter activity of both antisense transcripts is restricted to the aforementioned organs at all the analyzed developmental stages (Figure S1a).

To compare the expression domains of the sense and antisense genes we next generated and tested reporter lines for *UGT73C6* and, additionally, for its closest homolog *UGT73C5* (Figure 1a). Thus, we observed *UGT73C6* promoter activity in roots and cotyledons (Figure 1b) but not in young leaves where *NAT2*$_{UGT73C6}$ is detected (Figure S1b), suggesting a spatiotemporal separation of the expression of the sense and antisense genes in these organs. Analyses of the *UGT73C5* promoter activity revealed strong expression in cotyledons and roots, where its expression overlaps with those of *NAT1*$_{UGT73C6}$ and *UGT73C6*, and in developed leaves but not in young developing leaves where it is detected only in the tip region (Figure 1b; Figure S1b). The *NAT1*$_{UGT73C6}$ promoter was not active in flowers, whereas *NAT2*$_{UGT73C6}$ promoter activity was detected in stamen filaments and in silique pedicels (Figure S1c). The promoters of *UGT73C6* and *UGT73C5* were found to be active in anthers and silique pedicels, and in sepals, stamen filaments and style apex, respectively (Figure S1c).

Using quantitative reverse transcription-polymerase chain reaction (qRT-PCR), we also determined the expression of the sense and antisense genes at different time points (Figure 1c). The data suggest that the *NATs*$_{UGT73C6}$ (mainly *NAT2*$_{UGT73C6}$ according to the pattern detected with the reporter gene line showing activity in aerial organs) were expressed at all analyzed times. Except for the last time point included in the study (45 days after stratification; DAS), the transcript levels of *NATs*$_{UGT73C6}$ were observed to be higher than those of *UGT73C6* (Figure 1c). Consistent with these results, analysis of publicly available RNA-seq data showed that *NATs*$_{UGT73C6}$ were detected in a larger number of libraries (Figure S2a) and that their expression is higher than that of *UGT73C6* in all analyzed tissues and studied conditions (Figure S2b).

We identified the ends of the transcripts by circular 5′ RACE and conventional 3′ RACE. Sequence analysis of the clones containing the generated amplicons (Figure S3a,b) indicated a single transcription initiation site (TIS) for *UGT73C6* that matches the one reported in the databases (G_1), and five transcription termination sites (TTS), one major (G_{1668}) and four less frequent ones, located upstream of the reported TTS (Figure S3c,d). For *NATs*$_{UGT73C6}$, we found one main TTS, which coincides with that reported for *NAT2*$_{UGT73C6}$ (C_{-98}; Figure S3c,d) and three less frequent ones. Concerning the *NATs*$_{UGT73C6}$ 5′-ends, we identified three positions with a higher frequency (G_{1255}, U_{926} and C_{866}) and three less frequent ones (Figure S3c,d), suggesting the presence of different TIS, which is consistent with the existence of two transcripts and with the different localization of the promoter activity in the reporter lines. We confirmed these data by RT-PCR, and obtained successful amplification with all the primers flanking the TIS determined by 5′ RACE for *NATs*$_{UGT73C6}$ but not when using an oligo located close to the TIS reported in the database (Figure S3e).

Altogether, these results suggest that the promoters of both *NATs*$_{UGT73C6}$ transcripts are active, that the expression of the RNAs is developmentally regulated and that it occurs independently of the transcriptional activity of the *UGT73C6* gene in *cis* and that it is initiated at different TIS.

© 2022 The Authors.

1365313x, 2023, 3, Downloaded from https://onlinelibrary.wiley.com/doi/10.1111/tpj.16058 by Universite Paris-Saclay, Wiley Online Library on [05/04/2023]. See the Terms and Conditions (https://onlinelibrary.wiley.com/terms-and-conditions) on Wiley Online Library for rules of use; OA articles are governed by the applicable Creative Commons License

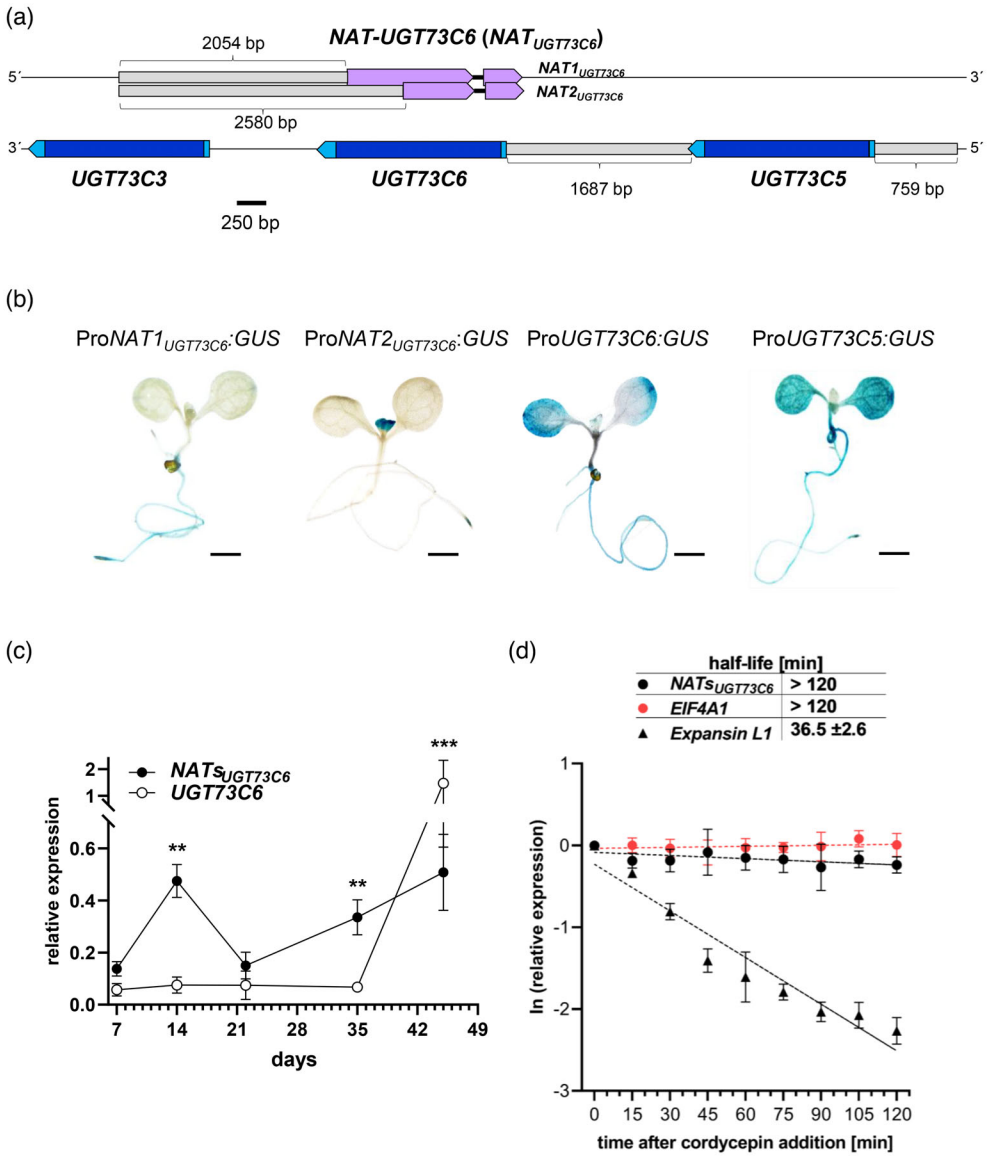

Figure 1. *NATs$_{UGT73C6}$* are stable and expressed at different developmental stages.
(a) Schematic showing the genomic arrangement of *UGT73C6*, its antisense gene *NAT$_{UGT73C6}$*, and the flanking genes *UGT73C3* and *UGT73C5*. Regions used as promoters to direct the expression of the *GUS* (*β-glucuronidase*) reporter gene are represented by gray boxes and their lengths indicated in base pairs (bp). Protein-coding genes and the natural antisense long non-coding RNAs (lncNATs) coding gene *NAT$_{UGT73C6}$* are indicated by blue and violet boxes, respectively. Untranslated regions (UTRs) are represented by light blue boxes and introns by thin black lines. The region is shown to scale.
(b) Histochemical analysis of GUS activity in 7-day-old seedlings grown on plates under long days (LDs; 16 h light/ 8 h dark cycle). Representative homozygous lines were chosen for detection of *NAT1$_{UGT73C6}$* (Pro*NAT1$_{UGT73C6}$:GUS*), *NAT2$_{UGT73C6}$* (Pro*NAT2$_{UGT73C6}$:GUS*), *UGT73C6* (Pro*UGT73C6:GUS*) and *UGT73C5* (Pro*UGT73C5:GUS*) promoter activity. Seedlings were stained overnight. Scale bars: 5 mm.
(c) Expression of *NATs$_{UGT73C6}$* and *UGT73C6* transcripts at various developmental stages. Seedlings and plants were grown under LD conditions. Quantitative reverse transcription-polymerase chain reaction (qRT-PCR) was performed on three–five independent biological replicates (pools of seedlings grown on plates for 7 and 14 days, and of 4–10 rosettes without floral stems from plants grown in soil for 22, 35 and 45 days). Dots represent means with standard deviation (SD). Expression levels were normalized to the reference gene *PP2A*. Statistically significant differences between both transcripts assessed by unpaired, two-tailed Student's *t*-test: $^{**}P \leq 0.01$; $^{***}P \leq 0.001$.
(d) Stability of *NATs$_{UGT73C6}$* RNAs in wild-type (Col-0) seedlings. Half-life ($t_{1/2}$, table) was calculated from degradation curves after cordycepin treatment (plot). Stable (*Eukaryotic translation initiation factor 4A1*, *EIF4A1*) and short-lived (*Expansin like 1*, *Expansin L1*) transcripts were included as controls. Values are means with SD from three independent experiments. *NATs$_{UGT73C6}$* includes both, *NAT1$_{UGT73C6}$* and *NAT2$_{UGT73C6}$*, transcripts.

NATs$_{UGT73C6}$ transcripts are alternatively spliced and stable

According to the TAIR10 database, the transcripts encoded by the *NAT$_{UGT73C6}$* gene contain an intron (Figure 1a). To determine the splicing pattern of the *NATs$_{UGT73C6}$* transcripts, we extracted total RNA from shoots of 9-day-old seedlings grown in long day (LD) conditions and

© 2022 The Authors.

1365313x, 2023, 3, Downloaded from https://onlinelibrary.wiley.com/doi/10.1111/tpj.16058 by Universite Paris-Saclay, Wiley Online Library on [05/04/2023]. See the Terms and Conditions (https://onlinelibrary.wiley.com/terms-and-conditions) on Wiley Online Library for rules of use; OA articles are governed by the applicable Creative Commons License

performed RT-PCR. The $NAT2_{UGT73C6}$ amplicon (Figure S4a) was cloned, and analysis of individual clones by colony PCR revealed the presence of inserts of different sizes (Figure S4b). Sequence analyses of the clones demonstrated that the $NAT2_{UGT73C6}$ transcripts consist of splicing variants in which half of the population retains the intron. The other half of the transcripts was shown to consist of three splicing variants with lengths of 1013, 1005 and 985 nucleotides, which are suggested to be generated using alternative, canonical splicing donor and acceptor sites (Figure S4c).

Considering that the subcellular localization of a lncRNA can provide clues to its function (Chen, 2016) and that lncRNAs localized in the nucleus are often unstable (Clark et al., 2012), we decided to determine the half-life of the $NATs_{UGT73C6}$ transcripts. With this aim in mind, we treated seedlings with cordycepin, an adenosine analog that induces termination of chain elongation when incorporated during RNA synthesis and quantified the transcript abundance at different time points, as previously described (Fedak et al., 2016). Stability determination based on degradation curves showed that the $NATs_{UGT73C6}$ transcripts have a relatively long half-life (> 120 min). Actually, the half-life of the $NATs_{UGT73C6}$ transcripts was found to be comparable, for the time analyzed, to that of the stable protein-coding transcript of a housekeeping gene (*Eukaryotic translation initiation factor 4A1*, *EIF4A*) and longer than that of a short-lived mRNA (*EXPANSIN-LIKE1*, *Expansin L1*; Figure 1d).

Overall, these data showed that the $NATs_{UGT73C6}$ transcripts are alternatively spliced and exhibit relatively high stability suggesting that it may function at the post-transcriptional level.

$NATs_{UGT73C6}$ downregulation leads to a reduction in the rosette area by decreasing leaf size and the number of mesophyll and epidermal cells

Considering a potential *trans*-activity of the $NATs_{UGT73C6}$ transcripts, we decided to analyze the effects of their downregulation. To achieve this, we first tested the earlier reported $ugt73c6_{ko}$ mutant line (SAIL_525_H07; Jones et al., 2003), which contains a T-DNA insertion at position 1440 downstream of the reported *UGT73C6* TIS (Figure S5a). The insertion generates a premature stop codon at position 472 leading to a protein that is truncated at its C-terminal end. qRT-PCR analysis confirmed that *UGT73C6* expression is strongly reduced in the mutant line. However, the $NATs_{UGT73C6}$ levels turned out to be unaltered (Figure S5b), suggesting that not only $NAT2_{UGT73C6}$ but also $NAT1_{UGT73C6}$ transcription may be initiated downstream of the T-DNA insertion. This idea was supported by the 5′ RACE results, as the first TIS detected at high frequency (G_{1255}) was located 187 nucleotides downstream of the insertion (Figure S3c,d). Due to the unaltered $NATs_{UGT73C6}$ levels, this line thus turned out to be unsuitable to study the effects of $NATs_{UGT73C6}$ downregulation.

Therefore, we generated two different collections of transgenic lines that, though the *35S* promoter, overexpress artificial microRNAs (amiRNAs; Carbonell et al., 2014) that specifically target both $NAT_{UGT73C6}$ transcripts (Figure S6a). In the first set of 15 independent homozygous lines, three were confirmed unambiguously to express the amiRNAs (Figure S6b). Interestingly, these plants showed a decrease in rosette size when compared with wild-type plants and with plants transformed with the empty vector. The $NATs_{UGT73C6}$ levels of these lines were found to show a reduction close to or higher than 50% (lines 1, 2 and 5; Figure S6c) as compared with the control plants when analyzed by qRT-PCR.

To quantify the observed phenotypic differences, we analyzed 25-day-old plants using available software (Easlon & Bloom, 2014). This confirmed the initial, macroscopic impression that lines indeed showed a reduced rosette area in comparison to the control plants (Figure S6e). With the second set of lines, which was generated afterwards, we first analyzed the levels of $NATs_{UGT73C6}$ in eight independent homozygous lines and identified one ($_{amiR}NATs_{UGT73C6}$-*10*) in which these were strongly reduced (Figure S6d). Interestingly, and consistent with the previous results, the plants from this line were the only ones that showed smaller rosettes when compared with wild-type plants and plants overexpressing amiRNAs targeting the *GUS* gene used as controls (Figure 2a,b). This phenotype was confirmed by further experiments (Figure 2c). Compiled data from each of these independent experiments showed that the average decrease in rosette area in lines with reduced $NATs_{UGT73C6}$ levels range between 13 and 20% (Figure 2c). In accordance with this, plants of the $_{amiR}NATs_{UGT73C6}$-*7* line and of the other lines ($_{amiR}NATs_{UGT73C6}$-*8* to -*9* and -*11* to -*14*), in which the $NATs_{UGT73C6}$ levels were not altered, showed no differences in rosette size (Figures 2c and S6f). In sum, we took these data as an indication that reduction in $NATs_{UGT73C6}$ transcripts leads to a decrease in the rosette area.

To exclude a potential effect of the UGT73C6 protein on the plant phenotype, we also performed rosette area measurements in the earlier mentioned $ugt73c6_{ko}$ line. The obtained data demonstrated that the absence of a functional UGT73C6 protein has no influence on the rosette size (Figure S5c), reinforcing the idea that the observed phenotypic changes result from the reduction of $NATs_{UGT73C6}$ levels.

To understand the contribution of the individual leaves to the overall change in rosette size, we determined the area of individual leaves from 30-day-old plants. Our results showed that all the leaves from the $_{amiR}NATs_{UGT73C6}$-*10* plants were smaller than those of the control plants, with differences that were statistically significant

© 2022 The Authors.

1365313x, 2023, 3, Downloaded from https://onlinelibrary.wiley.com/doi/10.1111/tpj.16058 by Universite Paris-Saclay, Wiley Online Library on [05/04/2023]. See the Terms and Conditions (https://onlinelibrary.wiley.com/terms-and-conditions) on Wiley Online Library for rules of use; OA articles are governed by the applicable Creative Commons License

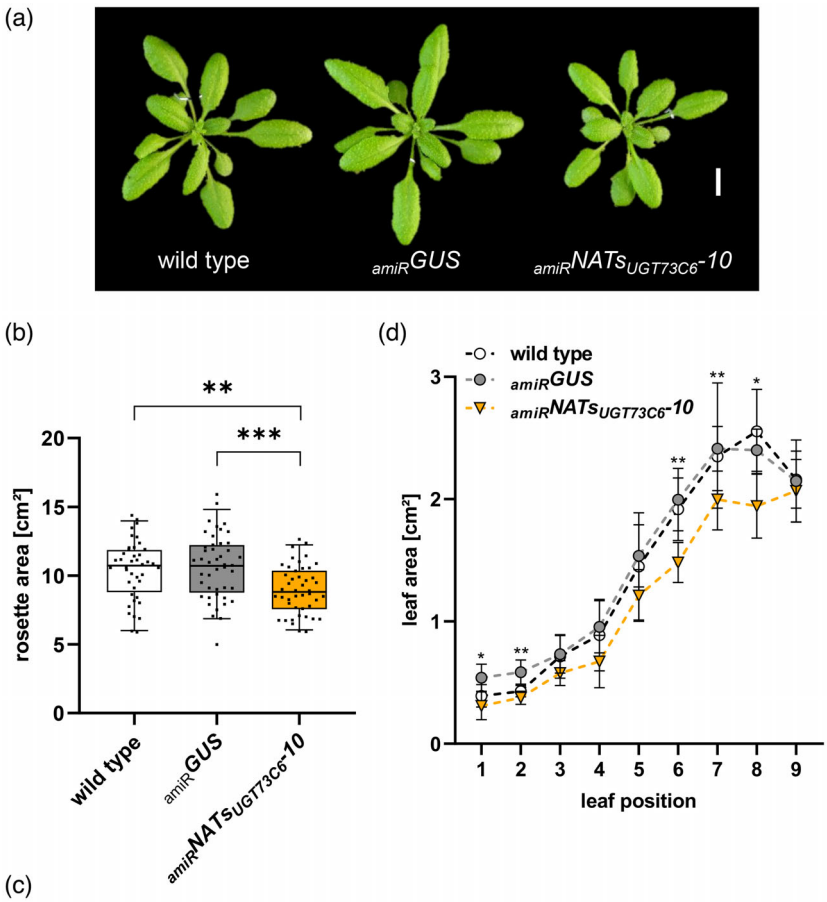

(c)

line	rosette area (% vs control)
$_{amiR}NATs_{UGT73C6}$-1	82.1 (±11.85)
$_{amiR}NATs_{UGT73C6}$-2	86.76 (±6.54)
$_{amiR}NATs_{UGT73C6}$-5	80.05 (±8.60)
$_{amiR}NATs_{UGT73C6}$-7	97.92 (±7.85)
$_{amiR}NATs_{UGT73C6}$-10	82.94 (±3.70)

Figure 2. Effects of *NATs$_{UGT73C6}$* downregulation on rosette area and leaf size.
(a) Representative pictures of 25-day-old wild-type (left), $_{amiR}$*GUS* control (center) and $_{amiR}$*NATs$_{UGT73C6}$-10* (right) plants. Scale bar: 1 cm.
(b) Rosette area of $_{amiR}$*NATs$_{UGT73C6}$-10* plants compared with wild-type and control plants expressing a *GUS*-specific amiRNA ($_{amiR}$*GUS*). Plants were grown under long day (LD) conditions and photographed at 25 days after sowing (DAS). Data compiled from two independent experiments including 20–25 plants per experiment are shown. Box plots show medians and interquartile ranges, whiskers extend from the 5th to the 95th percentile, and individual rosette values are shown as black dots. Statistically significant differences from wild-type assessed by one-way ANOVA and Tukey's honestly significant difference test: $^{**}P \leq 0.01$; $^{***}P \leq 0.001$.
(c) Quantification of rosette area reduction in plants from the $_{amiR}$*NATs$_{UGT73C6}$*-expressing lines compared with control plants (transformed with the empty vector or expressing $_{amiR}$*GUS*). Plants from the $_{amiR}$*NATs$_{UGT73C6}$-7* line, which shows wild-type levels of *NATs$_{UGT73C6}$*, were included as additional control. Numbers are means with standard deviation (SD) of the means from individual experiments expressed as a percentage compared with the control (100%). Data are from two ($_{amiR}$*NATs$_{UGT73C6}$-7*), three ($_{amiR}$*NATs$_{UGT73C6}$-1*, $_{amiR}$*NATs$_{UGT73C6}$-2* and $_{amiR}$*NATs$_{UGT73C6}$-5*) and four ($_{amiR}$*NATs$_{UGT73C6}$-10*) independent experiments, including 18–36 plants each.
(d) Area of individual leaves of 30-day-old wild-type, $_{amiR}$*GUS* and $_{amiR}$*NATs$_{UGT73C6}$-10* plants grown in soil under LD conditions. Graph shows mean and SD (n = 4–5) of areas from leaves 1–9. Statistically significant differences from wild-type assessed by two-tailed Student's *t*-test: $^{*}P \leq 0.05$; $^{**}P \leq 0.01$.

for leaves 1, 2, 6, 7 and 8 (Figure 2d). In a second experiment, we quantified the growth of individual leaves over time. We observed that the leaves from plants of the $_{amiR}$*NATs$_{UGT73C6}$-10* line were smaller at all time points analyzed (Figure S6g; Table S1), and that the differences were maintained even after leaf growth was completed

© 2022 The Authors.

1365313x, 2023, 3, Downloaded from https://onlinelibrary.wiley.com/doi/10.1111/tpj.16058 by Universite Paris-Saclay, Wiley Online Library on [05/04/2023]. See the Terms and Conditions (https://onlinelibrary.wiley.com/terms-and-conditions) on Wiley Online Library for rules of use; OA articles are governed by the applicable Creative Commons License

(e.g. leaves 1, 2, 3 and 4; Figure S6g). These results suggested that a reduction in size of the individual leaves was responsible for the smaller rosette area in the lines with reduced $NATs_{UGT73C6}$ levels.

We next wanted to understand whether the observed phenotype of the lines with downregulated $NATs_{UGT73C6}$ levels was possibly caused by changes in cell proliferation or cell expansion. For this purpose, we determined the cell size of palisade mesophyll and abaxial epidermal cells from the tip and the bottom regions of leaf 6 from $_{amiR}NATs_{UGT73C6}$-*10* and from the control ($_{amiR}GUS$) plants. Combined data including the cells from both leaf regions showed no differences in mesophyll cell size, but a statistically significant increase in epidermal cell area in the $_{amiR}NATs_{UGT73C6}$-*10* line (Figure 3b). Using these data, we estimated the total number of cells by dividing the determined total area of the individual leaves (Figure 3a) by the average cell area of each cellular type (Figure 3c). Results of these estimations showed that the total number of both cell types was significantly lower in the lines where the $NATs_{UGT73C6}$ levels had been reduced by the amiRNA knockdown approach (Figure 3c,d).

These data suggest that the smaller size of leaf 6 of the $_{amiR}NATs_{UGT73C6}$-*10* plants is mainly due to a decrease in cell number. Considering that in this line all leaves were found to be smaller than those of the control plants, we explained the reduction in rosette area by a reduction of the number of cells in each leaf. This idea was supported by the fact that in the plants with regulated $NATs_{UGT73C6}$ levels the estimated reduction of cell number (about 20% if both cell types are considered) correlated closely with the observed reduction in rosette area (17%; Figures 2c and 3d, respectively).

Overexpression of $NAT1_{UGT73C6}$ or $NAT2_{UGT73C6}$ induces an increase in rosette size

Considering that the previously described phenotype was a consequence of $NATs_{UGT73C6}$ downregulation, we now

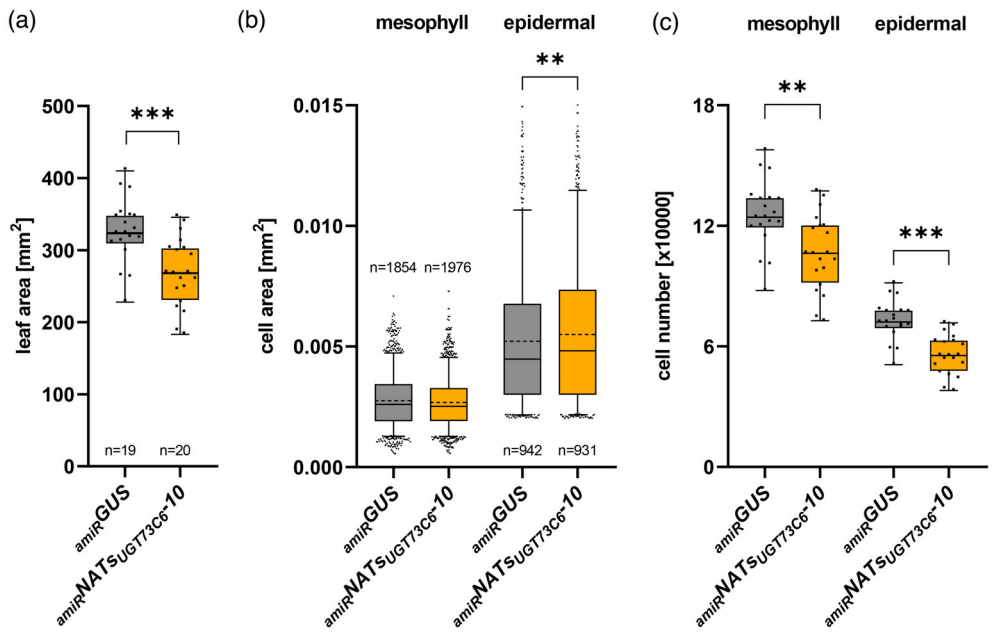

(d)

	$_{amiR}GUS$	$_{amiR}NATs_{UGT73C6}$-*10*
palisade mesophyll cells	125596 (±22371) (100%)	104355 (±18283) (83.1%)
abaxial epidermal cells	64254 (±11445) (100%)	48794 (±8549) (75.9%)

Figure 3. $NATs_{UGT73C6}$ downregulation has a negative effect on leaf cell number.
(a) Leaf area, (b) mesophyll and epidermal cell area, and (c) estimated number of mesophyll and epidermal cells on leaf 6 of 35-day-old $_{amiR}NATs_{UGT73C6}$-*10* and control ($_{amiR}GUS$) plants. Box plots show medians (solid line) and interquartile ranges, whiskers extend from the 5th to the 95th percentile. Dots represent individual values (a, c). In (b) the dotted lines and filled dots indicate the average cell area and outliers, respectively. Unpaired, two-tailed Student's *t*-test was applied for leaf area and cell number estimation, and one-way ANOVA followed by Tukey's honestly significant difference test for cell area. Statistical differences from the control: $^{**}P \leq 0.01$; $^{***}P \leq 0.001$. *n* indicates the number of leaves (a) or cells (b) measured.
(d) Estimated total number of cells on leaf 6 of 35-day-old $_{amiR}NATs_{UGT73C6}$-*10* and control ($_{amiR}GUS$) plants. Values are means with standard deviation of means from individual leaves ($n = 19$–20) and percentages compared with control (in brackets).

© 2022 The Authors.

1365313x, 2023, 3, Downloaded from https://onlinelibrary.wiley.com/doi/10.1111/tpj.16058 by Universite Paris-Saclay, Wiley Online Library on [05/04/2023]. See the Terms and Conditions (https://onlinelibrary.wiley.com/terms-and-conditions) on Wiley Online Library for rules of use; OA articles are governed by the applicable Creative Commons License

performed an experiment to determine if an increase of the $NATs_{UGT73C6}$ levels would lead to the opposite phenotype. For this purpose, we generated transgenic lines expressing each of the $NATs_{UGT73C6}$ under the control of the *35S* promoter. Several independent homozygous lines were selected (four overexpressing $NAT1_{UGT73C6}$ and four overexpressing $NAT2_{UGT73C6}$; Figure S7a,b) and rosette area determination was performed as described before. In all cases, plants from transgenic lines overexpressing the $NATs_{UGT73C6}$ sequences showed a small but significant increase in rosette size compared with control plants (Figure 4). Analyses from at least three independent experiments confirmed that overexpression of either $NAT1_{UGT73C6}$ or $NAT2_{UGT73C6}$ leads to an increase in rosette size, suggesting that, indeed, high levels of $NATs_{UGT73C6}$ transcripts determine this phenotype (Figure 4c). While lines overexpressing $NAT1_{UGT73C6}$ showed an increase of the rosette size ranging between 10 and 23%, these values were slightly higher in lines overexpressing $NAT2_{UGT73C6}$ (14–32%; Figure 4c). If all lines were considered, the average rosette increase was 14.65% (± 5.52%) for *NAT1-UGT73C6* and 22% (± 7.47%) for *NAT2UGT73C6*. Plants overexpressing *UGT73C5* included as a control showed the reported BR-deficiency phenotypes and a strong reduction (more than 40%) in rosette area (Figure 4a,c).

To determine the contribution of individual leaves to the changes in rosette area, we dissected and measured leaves from 30-day-old overexpressing $NAT2_{UGT73C6}$ and wild-type plants. Our analysis revealed that leaves of plants overexpressing $NAT2_{UGT73C6}$ (*OE-*$NAT2_{UGT73C6}$*-6*, a new generated line with high $NAT2_{UGT73C6}$ expression levels; Figure S9) were indeed larger than those of the control plants, showing statistically significant differences for leaves 1, 2, 3, 5 and 7 (Figure 4d). In addition, we quantified individual leaf growth by measuring leaf size at different time points. The analysis of the growth curve showed that the area of the individual leaves of the overexpression line was larger than that of the corresponding leaves of the control plants (Figure S7c; Table S2). Furthermore, we observed that the size differences also remained when leaf development was completed, suggesting that these differences did not result from a faster growth of the $NAT2_{UGT73C6}$ overexpression line.

Altogether, these data support the idea that overexpression of $NATs_{UGT73C6}$ induces an increase in the size of the individual leaves and thus an enlargement of the rosette area.

Increase in rosette area is caused by a *bona fide* lncRNA activity of the $NATs_{UGT73C6}$

According to the current definition, lncRNAs should not contain ORFs encoding peptides of more than 70 amino acids (Ben Amor et al., 2009). As already explained above, most of the ORFs predicted in the $NATs_{UGT73C6}$ encode less than 30 amino acids. However, $NAT1_{UGT73C6}$ and $NAT2_{UGT73C6}$ encode for a 103-amino-acid-long polypeptide, peptide 3 (Figure S8a). Therefore, it was important to understand whether the phenotypes observed in the knockdown and overexpression lines were associated with activities of the peptides or with the action of $NATs_{UGT73C6}$ as *bona fide* lncRNAs.

As overexpression of either $NATs_{UGT73C6}$ causes a similar phenotype in the transgenic plants, we decided to perform the following experiments solely with $NAT2_{UGT73C6}$. Thus, we generated C-terminal GFP-fusion constructs in which the stop codons of the four ORFs present in $NAT2_{UGT73C6}$ were removed by site-directed mutagenesis (Figure S8b; Supporting Figures Information) and, subsequently, performed transient expression assays in *Nicotiana benthamiana* (Supporting Figures Information). Confocal laser-scanning microscopy analysis and Western blot detection showed that three out of the four ORFs are translated from the constructs containing the upstream $NAT2_{UGT73C6}$ sequences, whereas absence of signal was observed in the areas infiltrated with *35S:NAT2-ORF4-GFP* (Figure S8c,d).

Based on these results and to determine whether the phenotypes that we observed during the overexpression of $NAT2_{UGT73C6}$ were due to a *bona fide* activity of the RNA, we generated a set of transgenic lines in which we substituted the start codons of ORFs 1–3 by a CCC codon encoding proline (Figure 5a). We identified four independent homozygous lines that overexpressed the mutated, non-peptide-coding sequence of $NAT2_{UGT73C6}$ ($_{mut}NAT2_{UGT73C6}$) at high levels (*OE-*$_{mut}NAT2_{UGT73C6}$ lines 1–4; Figure S9), and assessed the impact of this variant on the identified phenotype. Interestingly, we found that in all the *OE-*$_{mut}NAT2_{UGT73C6}$ lines, the rosette area was increased in comparison with the Col-0 wild-type controls (Figure 5b). Another important finding was that the values obtained in rosette area measurements with these lines correlated closely with those obtained in lines overexpressing the unmodified (wild-type) $NAT2_{UGT73C6}$ sequence (Figure 5b), two of which (*OE-*$NAT2_{UGT73C6}$ lines 5 and 6) were generated *de novo* for this comparison.

Overall, these data indicate that, as with wild-type $NAT2_{UGT73C6}$, overexpression of the $_{mut}NAT2_{UGT73C6}$ variant leads to an increase in rosette area, suggesting that the observed phenotype depends on properties related to the RNA molecule itself.

Above, we reported that the downregulation of $NATs_{UGT73C6}$ transcripts leads to a reduction in the number of mesophyll and epidermal cells in leaves (Figure 3c), while $NATs_{UGT73C6}$ overexpression generates an increase of the rosette area. In view of this scenario, we decided to quantify cell size in leaf 6 of 35-day-old wild-type plants and plants overexpressing $NAT2_{UGT73C6}$ (*OE-*$NAT2_{UGT73C6}$*-6*) and the $_{mut}NAT2_{UGT73C6}$ variant (*OE-*$_{mut}NAT2_{UGT73C6}$*-3*). For

© 2022 The Authors.

1365313x, 2023, 3, Downloaded from https://onlinelibrary.wiley.com/doi/10.1111/tpj.16058 by Universite Paris-Saclay, Wiley Online Library on [05/04/2023]. See the Terms and Conditions (https://onlinelibrary.wiley.com/terms-and-conditions) on Wiley Online Library for rules of use; OA articles are governed by the applicable Creative Commons License

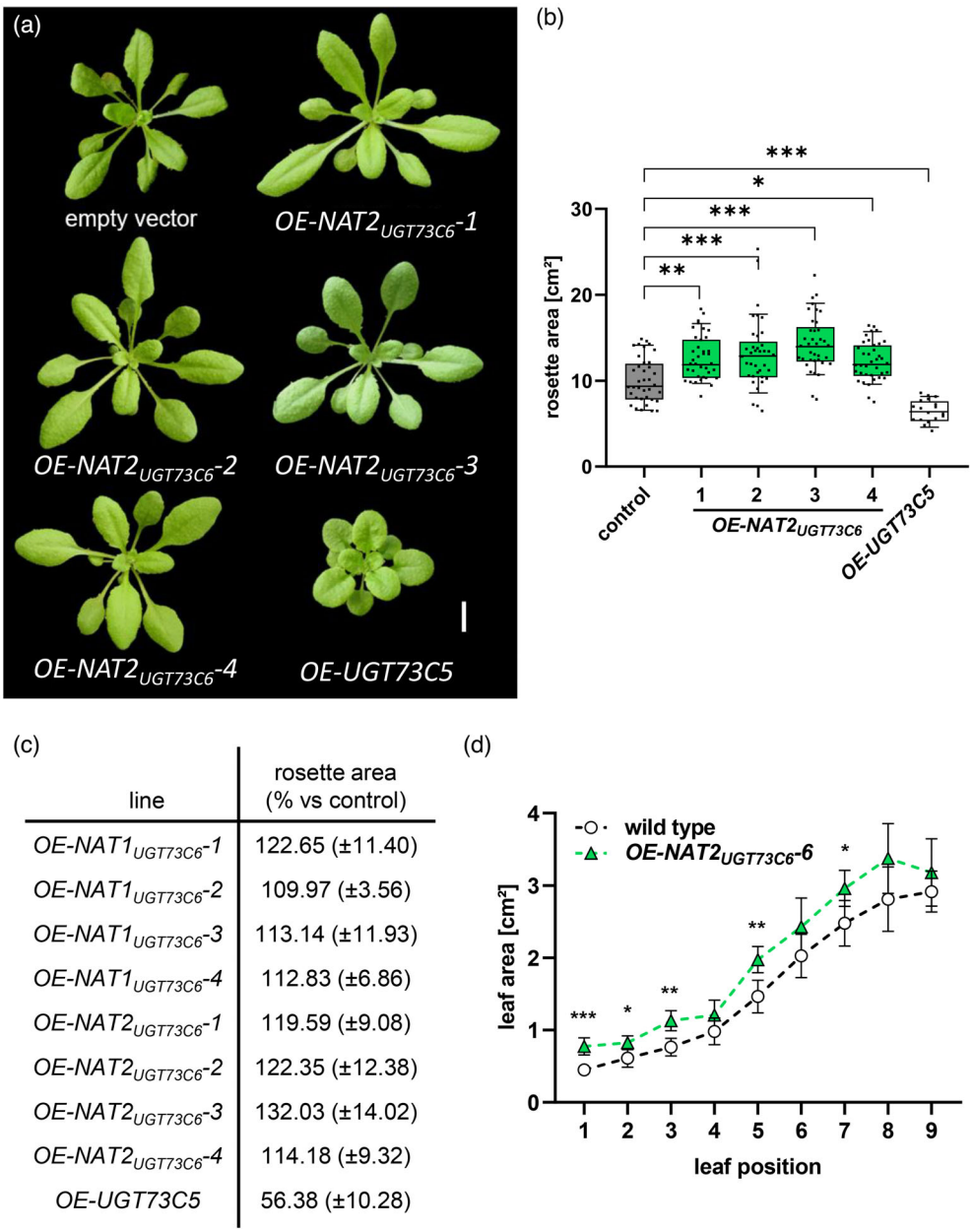

line	rosette area (% vs control)
OE-NAT1$_{UGT73C6}$*-1*	122.65 (±11.40)
OE-NAT1$_{UGT73C6}$*-2*	109.97 (±3.56)
OE-NAT1$_{UGT73C6}$*-3*	113.14 (±11.93)
OE-NAT1$_{UGT73C6}$*-4*	112.83 (±6.86)
OE-NAT2$_{UGT73C6}$*-1*	119.59 (±9.08)
OE-NAT2$_{UGT73C6}$*-2*	122.35 (±12.38)
OE-NAT2$_{UGT73C6}$*-3*	132.03 (±14.02)
OE-NAT2$_{UGT73C6}$*-4*	114.18 (±9.32)
OE-UGT73C5	56.38 (±10.28)

Figure 4. *NATs*$_{UGT73C6}$ overexpression increases rosette area.
(a) Pictures from 25-day-old control (transformed with the empty vector) and *NAT2*$_{UGT73C6}$-overexpressing (*OE*) plants. Representative plants corresponding to four independent homozygous lines are shown. Plants overexpressing *UGT73C5* were included for comparison. Scale bar: 1 cm.
(b) Rosette area of *NAT2*$_{UGT73C6}$*-OE* plants compared with control plants transformed with the empty vector. Plants were grown in soil under long day (LD) conditions and photographed at 25 days after sowing (DAS). Data compiled from two independent experiments including 18 and 19 plants, respectively. Plants overexpressing *UGT73C5* (n = 18) were included as controls in one experiment. Box plots show medians and interquartile ranges, whiskers extend from the 5th to the 95th percentile, and individual values are shown as black dots. Statistically significant differences from control plants assessed by one-way ANOVA and Tukey's honestly significant difference test: *$P \leq 0.05$; **$P \leq 0.01$; ***$P \leq 0.001$.
(c) Quantification of the rosette area in homozygous lines overexpressing *NAT1*$_{UGT73C6}$ or *NAT2*$_{UGT73C6}$ compared with a line transformed with the empty vector. Numbers are means with standard deviation (SD) of means from individual experiments expressed as percentage of the control (100%). Data are from three independent experiments including 17–20 plants each.
(d) Area of individual leaves of 30-day-old wild-type and *NAT2*$_{UGT73C6}$-overexpressing (*OE-NAT2*$_{UGT73C6}$*-6*) plants grown in soil under LD conditions. The graph shows mean and SD (n = 4–5) of the areas of leaves 1–9. Statistically significant differences from wild-type assessed by two-tailed Student's t-test: *$P \leq 0.05$; **$P \leq 0.01$; ***$P \leq 0.001$.

© 2022 The Authors.

1365313x, 2023, 3, Downloaded from https://onlinelibrary.wiley.com/doi/10.1111/tpj.16058 by Universite Paris-Saclay, Wiley Online Library on [05/04/2023]. See the Terms and Conditions (https://onlinelibrary.wiley.com/terms-and-conditions) on Wiley Online Library for rules of use; OA articles are governed by the applicable Creative Commons License

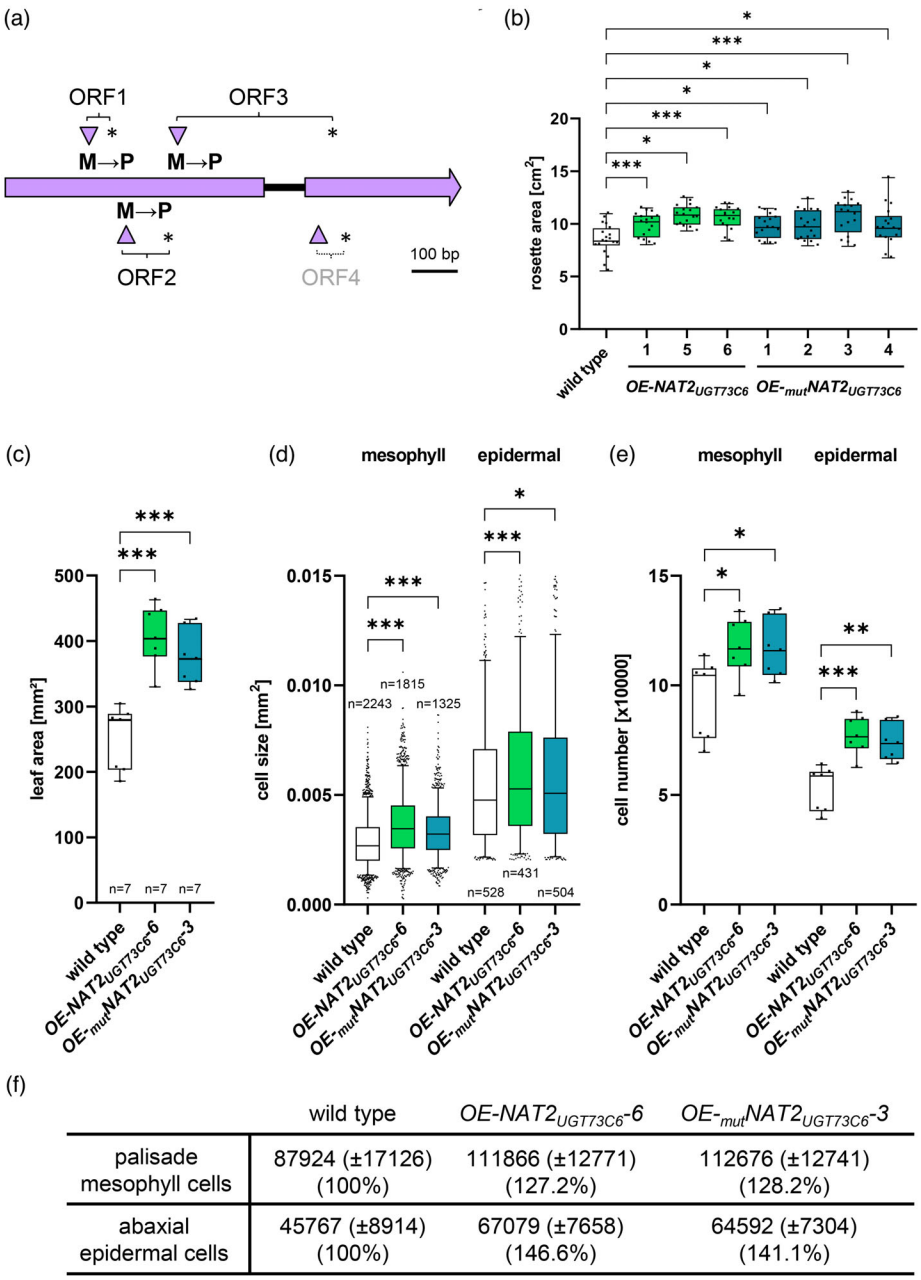

	wild type	*OE-NAT2*$_{UGT73C6}$*-6*	*OE-*$_{mut}$*NAT2*$_{UGT73C6}$*-3*
palisade mesophyll cells	87924 (±17126) (100%)	111866 (±12771) (127.2%)	112676 (±12741) (128.2%)
abaxial epidermal cells	45767 (±8914) (100%)	67079 (±7658) (146.6%)	64592 (±7304) (141.1%)

Figure 5. Overexpression of *NAT2*$_{UGT73C6}$ or its mutant variant, *$_{mut}$NAT2*$_{UGT73C6}$ increases rosette and leaf area, and the number of epidermal and mesophyll cells.

(a) Schematic of *$_{mut}$NAT2*$_{UGT73C6}$, the *NAT2*$_{UGT73C6}$ variant generated by site-directed mutagenesis that lacks the ability to encode peptides. Methionine to proline (M → P) changes introduced by site-directed mutagenesis of start codons at positions 198 (ORF1), 289 (ORF2) and 405 (ORF3) are shown. Arrowheads and asterisks indicate start and stop codons, respectively.

(b) Rosette area of wild-type plants and plants overexpressing *NAT2*$_{UGT73C6}$ (*OE-NAT2*$_{UGT73C6}$) or *$_{mut}$NAT2*$_{UGT73C6}$ (*OE-*$_{mut}$*NAT2*$_{UGT73C6}$). Plants were grown in soil under long day (LD) conditions and photographed at 25 days after sowing (DAS). Shown are data from one representative experiment including 19 and 17 plants of the wild-type control and transgenic lines, respectively. Statistically significant differences from control plants assessed by one-way ANOVA and Tukey's honestly significant difference test: $*P \leq 0.05$; $***P \leq 0.001$.

(c) Leaf area, (d) mesophyll and epidermal cell area, and (e) estimated number of mesophyll and epidermal cells on leaf 6 of 35-day-old control plants (wild-type) and plants overexpressing *NAT2*$_{UGT73C6}$ (*OE-NAT2*$_{UGT73C6}$*-6*) or *$_{mut}$NAT2*$_{UGT73C6}$ (*OE-*$_{mut}$*NAT2*$_{UGT73C6}$*-3*). Dots represent individual values in (c) and (e). Dotted lines and filled dots in (d) indicate average cell area and outliers, respectively. Statistically significant differences: $*P \leq 0.05$; $**P \leq 0.01$; $***P \leq 0.001$ [assessed by two-tailed Student's *t*-test for (c) and (e), and by one-way ANOVA and Tukey's honestly significant difference test for (d)]. *n* indicates the number of leaves (c) or cells (d) measured.

(f) Estimated total cell number on leaf 6 of 35-day-old wild-type, *OE-NAT2*$_{UGT73C6}$*-6* and *OE-*$_{mut}$*NAT2*$_{UGT73C6}$*-3* plants. Numbers are means with SD of means from individual leaves ($n = 7$). Percentages versus control (100%) are given in brackets.

Box plots show medians and interquartile ranges; whiskers extend from the 5th to the 95th percentile.

© 2022 The Authors.

1365313x, 2023, 3, Downloaded from https://onlinelibrary.wiley.com/doi/10.1111/tpj.16058 by Universite Paris-Saclay, Wiley Online Library on [05/04/2023]. See the Terms and Conditions (https://onlinelibrary.wiley.com/terms-and-conditions) on Wiley Online Library for rules of use; OA articles are governed by the applicable Creative Commons License

this purpose, we harvested leaves from representative plants and performed cell-size measurements of abaxial epidermal and mesophyll cells in the tip and in the bottom regions. Interestingly, however, mesophyll and epidermal cells of either the $NAT2_{UGT73C6}$- or the $_{mut}NAT2_{UGT73C6}$-overexpressing plants showed a statistically significant increase in area compared with the control (Figure 5d), suggesting that the observed differences in leaf size are, at least in part, also due to cell enlargement. Estimations of the total cell number based on the mean cell size (Figure 5d) and determined leaf area (Figure 5c) revealed a significant increase of both cell types in the $NAT2_{UGT73C6}$ and the $_{mut}NAT2_{UGT73C6}$ overexpressing lines (Figure 5e).

Thus, on the one hand, these data confirmed the earlier finding (Figures 3 and 4) showing that the presence and expression level of the $NATs_{UGT73C6}$ modulates cell number and, consequently, leaf and rosette size. On the other hand, we obtained some evidence that also an increase in cell size contributes to the $NATs_{UGT73C6}$-mediated phenotype.

Ectopic alteration of $NATs_{UGT73C6}$ expression does not affect the transcript levels of the *UGT73C6* sense gene or that of its closely related homolog *UGT73C5*

In an earlier report it has been proposed that in the UGT multigene family, lncNATs can modulate the expression of the sense gene and closely related genes acting in *trans* (Wang et al., 2006). Hence, we wanted to understand whether such a scenario also applies to the studied $NATs_{UGT73C6}$, the corresponding sense gene *UGT73C6* and its closest homolog *UGT73C5*.

The availability of the transgenic *A. thaliana* lines with altered $NATs_{UGT73C6}$ levels allowed us to quantify the expression of *UGT73C6* and *UGT73C5* in these lines. Surprisingly, we observed that *UGT73C6* and *UGT73C5* mRNA levels were not decreased in homozygous plants overexpressing $NAT1_{UGT73C6}$ or $NAT2_{UGT73C6}$ (Figure 6a; Figure S10). Consistently, we found that *UGT73C6* and *UGT73C5* expression was also not altered in lines with reduced $NATs_{UGT73C6}$ levels (Figure 6a; Figure S10).

Altogether, these results revealed that, at least in the natural host *A. thaliana*, ectopic changes in the expression of the $NATs_{UGT73C6}$ transcripts do not affect their complementary mRNAs and that the resulting leaf phenotype is not a consequence of significant changes in the expression of *UGT73C6* and *UGT73C5*.

BR treatment does not consistently affect the levels of $NATs_{UGT73C6}$ transcripts, and BR marker genes are not changed in line with altered $NATs_{UGT73C6}$ expression

Our data suggested that $NATs_{UGT73C6}$ have no direct effect on the expression of *UGT73C6*, an important player in BR homeostasis (Husar et al., 2011). To gain further insights into a possible role for the $NATs_{UGT73C6}$ in this context, we decided to analyze the gene responses to externally applied BR. To this end, we treated 8-day-old wild-type seedlings with 1 μM 24-epiBL, collected samples at different incubation times and determined gene expression levels by qRT-PCR. Consistent with a previous report (Husar et al., 2011), we found that expression of *UGT73C6* and *UGT73C5* was not significantly altered (Figure 6b). Moreover, we observed that the treatment also had little effect on $NATs_{UGT73C6}$ expression, with an increase in expression after 3 h, which, however, was not maintained after longer incubation periods (Figure 6b). Control genes analyzed to monitor the experimental conditions behaved as expected: i.e. expression of *CYTOCHROME P450 90B1* (*DWF4*), a gene repressed by BR application, was significantly decreased, while expression of *PHYB ACTIVATION-TAGGED SUPRESSOR 1* (*BAS1*), a catabolic gene induced under the same conditions, was significantly increased (Figure 6b). Further expression analyses at early time points revealed that neither $NATs_{UGT73C6}$ nor *UGT73C6* nor *UGT73C5* levels were affected after short periods of BR treatment (Figure S11a).

Thus, under the given conditions, the expression of $NATs_{UGT73C6}$ was not consistently altered in response to BR treatment.

Next, we considered it important to understand whether the phenotypes, which resulted from altered $NATs_{UGT73C6}$ levels, were caused by changes in the content of active BR. To address this, we determined, in line with altered $NATs_{UGT73C6}$ levels, the expression of *ROTUNDIFOLIA3* (*ROT3*), a BR biosynthetic gene, and *EXPANSIN 8* (*EXP8*), a BR-responsive gene of the expansin family (Goda et al., 2002). The results of these analyses showed that *ROT3* expression was not significantly affected when $NATs_{UGT73C6}$ were overexpressed or downregulated (Figure 6c, left). *EXP8* expression was reduced in all lines tested, including the $NATs_{UGT73C6}$ knockdown line, where the reduction was statistically significant but did not reach 50% (Figure 6c, right). In contrast, in lines overexpressing *UGT73C5*, *ROT3* expression was increased and *EXP8* levels were significantly reduced (Figure S11b), which was consistent with the described role of UGT73C5 in BR inactivation (Poppenberger et al., 2005).

Thus, these results suggest that active BR levels are not significantly changed in line with altered $NATs_{UGT73C6}$ expression and, consequently, are not associated with the observed phenotype.

Alteration of $NATs_{UGT73C6}$ expression leads to changes in *GRFs* transcript levels

Our results suggested that changes in $NATs_{UGT73C6}$ expression affect leaf and rosette size mainly by altering the number of mesophyll and epidermal cells. In the experiments with our promoter-GUS reporter lines we observed that $NAT2_{UGT73C6}$ is expressed in young leaves and particularly

© 2022 The Authors.

1365313x, 2023, 3, Downloaded from https://onlinelibrary.wiley.com/doi/10.1111/tpj.16058 by Universite Paris-Saclay, Wiley Online Library on [05/04/2023]. See the Terms and Conditions (https://onlinelibrary.wiley.com/terms-and-conditions) on Wiley Online Library for rules of use; OA articles are governed by the applicable Creative Commons License

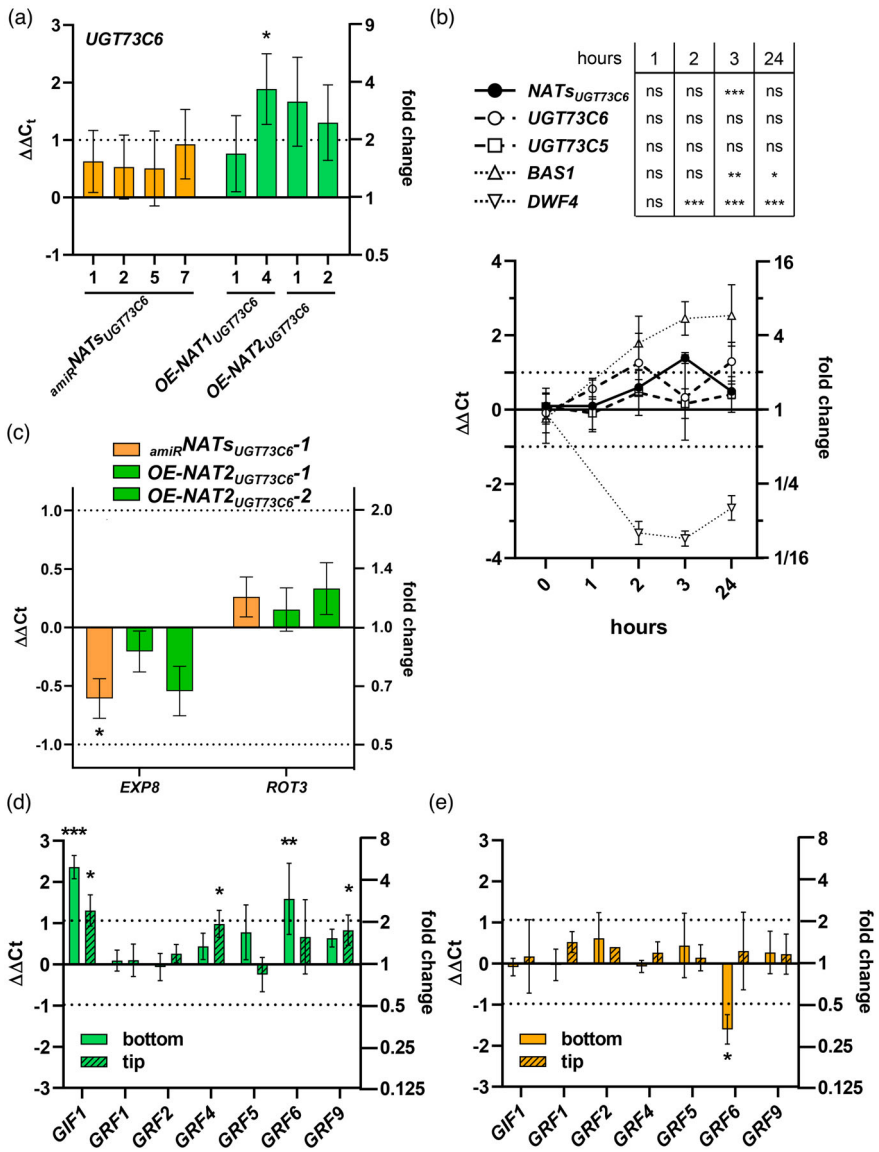

Figure 6. Levels of *GRFs* but not of *UGT73C6* or brassinosteroid (BR) marker genes are affected in line with altered *NATs$_{UGT73C6}$* expression.

(a) Expression of *UGT73C6* in line with reduced (*$_{amiR}$*) or increased (*OE*) *NATs$_{UGT73C6}$* levels. Bar graphs show $\Delta\Delta C_t$ [mean difference of ΔC_t between lines with modified long non-coding natural antisense transcripts (lncNATs) expression and control lines (ΔC_t $_{ami}$RNA expressing line or *NATs$_{UGT73C6}$*-overexpressing line – ΔC_t control line)] and standard error (SE) of mean differences of three independent biological replicates [pools of 14-day-old seedlings grown under long day (LD) conditions]. Statistically significant differences assessed by unpaired, two-tailed Student's *t*-test.

(b) Response of *NATs$_{UGT73C6}$*, *UGT73C6* and *UGT73C5* to BR treatment determined by quantitative reverse transcription-polymerase chain reaction (qRT-PCR). Seven-day-old seedlings were treated with either 1 μM 24-epi-brassinolide (24-epiBL) or dimethyl sulfoxide (DMSO; mock treatment), and samples were collected at the indicated time points. Compiled data from independent experiments including at least three biological replicates (pools of seedlings). Symbols indicate $\Delta\Delta C_t$ values [mean difference in ΔC_t between treated and control samples (ΔC_t 24-epiBL-treated – ΔC_t DMSO-treated samples)] and SE of mean differences. Expression analysis of BL-responsive genes *CYTOCHROME P450 90B1* (*DWF4*) and *PHYB ACTIVATION-TAGGED SUPRESSOR 1* (*BAS1*) was included to monitor treatment efficacy. Results of data analysis using multiple *t*-test are indicated in the upper panel.

(c) Expression of the BR-responsive genes *ROTUNDIFOLIA3* (*ROT3*) and *EXPANSIN 8* (*EXP8*) in transgenic lines with reduced (amiR) or increased (OE) *NATs$_{UGT73C6}$* expression. Bar graph indicates $\Delta\Delta C_t$ [mean difference of ΔC_t between lines with altered *NATs$_{UGT73C6}$* expression and control lines (ΔC_t $_{ami}$RNA expressing line or *NATs$_{UGT73C6}$*-overexpressing line – ΔC_t control line)] and SE of mean differences of three biological replicates (independent pools of 10-day-old seedlings grown under LD conditions). Statistically significant differences assessed by unpaired, two-tailed Student's *t*-test.

(d, e) *GIF1* and *GRFs* expression analysis in the tip and bottom regions of leaf 3 from lines with increased (*OE-NAT2$_{UGT73C6}$-6*) or reduced (*$_{amiR}$NATs$_{UGT73C6}$-10*) *NATs$_{UGT73C6}$* expression. Bar graphs show $\Delta\Delta C_t$ values [mean difference in ΔC_t between lines with altered *NATs$_{UGT73C6}$* expression and controls (ΔC_t in *NAT2-$_{UGT73C6-6}$* or *$_{amiR}$NATs$_{UGT73C6}$-10* – ΔC_t in control)] and SE of mean differences from three–four biological replicates (independent pools of leaf sections from 12-day-old seedlings grown under LD conditions). Smooth and dashed bars indicate values for bottom and tip regions, respectively. Statistically significant differences assessed by unpaired, two-tailed Student's *t-test*.

Expression levels were normalized to the reference genes *PP2A* (a, d, e) or *GAPC2* (b, c). Dotted lines indicate a twofold change (a, b, d, e). *$P \leq 0.05$; **$P \leq 0.01$; ***$P \leq 0.001$. *P*-values greater than 0.05 ($P > 0.05$) are indicated as non-significant (ns) (b) or with the absence of asterisks (a, c–e).

© 2022 The Authors.

1365313x, 2023, 3, Downloaded from https://onlinelibrary.wiley.com/doi/10.1111/tpj.16058 by Universite Paris-Saclay, Wiley Online Library on [05/04/2023]. See the Terms and Conditions (https://onlinelibrary.wiley.com/terms-and-conditions) on Wiley Online Library for rules of use; OA articles are governed by the applicable Creative Commons License

in the bottom region (Figures S1a,b and S12a), and that its expression decreases during leaf development (Figure S1b). Interestingly, this pattern matches that of the members of the *GRF* family of transcriptional regulators, which are strongly expressed in actively growing and developing tissues (Rodriguez et al., 2010). GRFs and the transcriptional coactivator ANGUSTIFOLIA 3/GRF-INTERACTING FACTOR 1 (AN3/GIF1), which physically interacts with six of the nine proteins encoded by the *GRF* family members, are key regulators of leaf growth by modulating cell proliferation (Vercruysse et al., 2020). The progression of leaf development is further controlled by miR396, which regulates the expression of seven of the nine *GRFs* at the post-transcriptional level (Jones-Rhoades & Bartel, 2004; Liu et al., 2009; Rodriguez et al., 2010). In accord with this, we identified a potential binding site for miR396 in the $NATs_{UGT73C6}$ sequence (Figure S12b), supporting the idea that $NATs_{UGT73C6}$ transcripts may have the potential to act as endogenous target mimics. In this way, alteration in $NATs_{UGT73C6}$ expression could cause changes in *GRFs* levels.

To address this hypothesis, we decided to determine the transcript levels of *GRFs* and *GIF1* in the bottom and tip regions of young developing leaves of transgenic lines with altered $NATs_{UGT73C6}$ expression. For this purpose, we dissected leaf 3 from 12-day-old seedlings grown on plates. We selected this time point because it has been previously reported that both cell proliferation and expansion continue to occur in the bottom and the tip regions of the leaf, respectively. Analyses of the obtained qRT-PCR data showed that the levels of several GRF mRNAs, including those of *GRF4*, *6* and *9*, were increased in the line overexpressing $NAT2_{UGT73C6}$ (Figure 6d). In addition, we detected a statistically significant increase of *GIF1* levels in both leaf regions (Figure 6d). On the other hand, in $_{amiR}NATs_{UGT73C6}$-*10*, the line with reduced $NATs_{UGT73C6}$ levels, we detected a statistically significant reduction in *GRF6* transcripts at the leaf bottom (Figure 6e). Notably, *GRF6* was found to be the only analyzed *GRF* whose expression levels were changed in the lines where $NAT2_{UGT73C6}$ transcripts were overexpressed or downregulated. Interestingly, we observed here a positive correlation: i.e. in comparison to the appropriate controls, the *GRF6* level was found to be increased when $NAT2_{UGT73C6}$ was overexpressed, while it was decreased when $NATs_{UGT73C6}$ were downregulated (Figure 6d,e). These data indicate a mechanism possibly involving members of the GRF/GIF module, and in particular GRF6.

Altogether, these results suggest that $NATs_{UGT73C6}$ modulate *GIF1* and *GRFs* levels, which in turn affect cell proliferation leading to changes in leaf size and rosette area.

DISCUSSION

Here we present the functional characterization of two lncNATs transcribed from a gene overlapping the *UGT73C6* gene of *A. thaliana*. First, by using reporter lines and qPCR analysis, we confirmed that both $NATs_{UGT73C6}$ are expressed and that the promoters are active in different organs. Furthermore, we demonstrated that the expression of the $NATs_{UGT73C6}$ is developmentally controlled and occurs independently of the presence of the sense gene in *cis*. Similar observations have been made previously with other lncNATs in plants (Fedak et al., 2016; Jabnoune et al., 2013), reinforcing the idea that the identified lncNATs are functionally relevant and do not correspond to transcriptional 'background noise' resulting from sense gene expression.

Several of the earlier characterized lncNATs from plants act in *trans* on their targets when ectopically overexpressed. These examples include *asHSFB2a*, which controls gametophyte development (Wunderlich et al., 2014), and *FLORE*, which modulates the onset of flowering (Henriques et al., 2017) in *Arabidopsis*, and *cis-NATPHO1;2*, which regulates phosphate homeostasis in rice (Jabnoune et al., 2013). We found the half-life of $NATs_{UGT73C6}$ to be comparable to that of a canonical mRNA, a feature indeed that suggests a *trans*-acting function.

In our studies, we demonstrate that changes in $NATs_{UGT73C6}$ expression levels, which were achieved by post-transcriptional downregulation by amiRNAs or overexpression under the control of the strong *35S* promoter, result in mild but consistent phenotypes in which the size of individual leaves and, consequently, rosette area was affected (Figures 2 and 4). In line with a $NATs_{UGT73C6}$ downregulation close to 50% the rosette area was reduced by almost 20% in comparison to controls where the $NATs_{UGT73C6}$ transcript levels were unaffected. Interestingly, reductions in size were observed in all leaves and were also maintained in fully developed leaves, indicating that this phenotype is not a consequence of delayed growth. On the other hand, overexpression of either of the $NATs_{UGT73C6}$ transcripts resulted in plants with increased rosette area. The same phenotype was detectable when full-length, mutated non-peptide-coding variants of $NAT2_{UGT73C6}$ were overexpressed. The later observations were important, especially considering that both $NATs_{UGT73C6}$ contain several ORFs and that one of them codes for a 103-amino-acid-long peptide when translated from the unspliced $NATs_{UGT73C6}$ variant. These results support the conclusion that the phenotype identified is due to the activity of the RNA molecules themselves, which thus function as *bona fide* lncRNAs.

Our analyses at the cellular level showed that in the line in which $NATs_{UGT73C6}$ were downregulated there was no significant difference in mesophyll cell size and that the size of the abaxial epidermal cells was slightly increased. Accordingly, both observations could not explain the reduction in leaf size. However, when estimating the total cell number, we observed a clear decrease for both cell

© 2022 The Authors.

1365313x, 2023, 3, Downloaded from https://onlinelibrary.wiley.com/doi/10.1111/tpj.16058 by Universite Paris-Saclay, Wiley Online Library on [05/04/2023]. See the Terms and Conditions (https://onlinelibrary.wiley.com/terms-and-conditions) on Wiley Online Library for rules of use; OA articles are governed by the applicable Creative Commons License

types, suggesting that cell proliferation is affected. On the other hand, in line with increased expression of the wild-type *NAT2*$_{UGT73C6}$ or of the mutated *NAT2*$_{UGT73C6}$ variant, the cell area of both cell types was found to be increased. While these size differences again did not explain the observed changes in leaf area, we obtained further data indicating that the cell number is increased in the overexpression lines. Thus, in sum our data suggest that the main differences in leaf size that were observed in line with altered *NATs*$_{UGT73C6}$ levels result from changes in cell proliferation.

As explained above, NATs may control the expression of a sense transcript in *cis* or in *trans*. Given the high sequence similarity of *UGT73C*-subfamily members, we originally assumed that the *NATs*$_{UGT73C6}$ would regulate the expression of *UGT73C6* and/or other closely related *UGTs*, as it has been reported for *FLORE*, which represses multiple *CDFs* (*CYCLING DOF FACTORS*) in *cis* and *trans* (Henriques et al., 2017). However, our data show that overexpression of *NATs*$_{UGT73C6}$ did not reduce the transcript levels of either *UGT73C6* or its closest homolog *UGT73C5*. These results are congruent with those reported by Deforges and coworkers who obtained transgenic lines with high overexpression of *cis*-NATs in which sense gene expression remained unaffected (Deforges et al., 2019). On the other hand, our data contrast with the 'Yin-Yang' mechanism proposed for the pair formed by *HSFB2a* and *asHSFB2a*, in which overexpression of either member of the pair leads to knockdown of the other (Wunderlich et al., 2014). Consistently, post-transcriptional downregulation of *NATs*$_{UGT73C6}$ by amiRNAs was found to have no effect on the level of *UGT73C6* or *UGT73C5* transcripts, indicating that *NATs*$_{UGT73C6}$ do not modulate, at least when their activity in *trans* is considered, the expression of these genes or the levels of their transcripts. Unfortunately, the *NATs*$_{UGT73C6}$ TISs locate within the coding sequence of *UGT73C6* (Figure S3c–e) making it difficult, if not impossible, to study their effect on *UGT73C6* expression in *cis*. Therefore, we cannot exclude potential *cis* effects of *NATs*$_{UGT73C6}$ transcription on *UGT73C6* expression. However, our data strongly suggest that the *NATs*$_{UGT73C6}$ are not involved in BR homeostasis. Furthermore, no link between *NATs*$_{UGT73C6}$ and hormone levels could be established.

By contrast, our data suggest that the observed, distinct phenotypes are a direct consequence of the activities of the *NATs*$_{UGT73C6}$ transcripts. Based on this premise, we decided to analyze the expression of other potential targets. Considering: (i) the observed changes in the number of cells in response to the alteration of the expression of *NATs*$_{UGT73C6}$ (Figures 3 and 5); (ii) the pattern of *NAT2*$_{UGT73C6}$ promotor activity, which is mainly detected at the bottom region of young developing leaves (Figure S12a); and (iii) the presence of a potential binding site with partial complementarity to miR396 in the *NATs*$_{UGT73C6}$ sequence (Figure S12b), we focused our analysis on the members of the *GRF* family, which, together with GIF1, are crucial for cell number determination in leaves (Vercruysse et al., 2020). Members of the *GIF* and *GRF* gene families are predominantly expressed at the bottom region of young leaves (Rodriguez et al., 2010), and the levels of most of the *GRF* family members are regulated by miR396 (Jones-Rhoades & Bartel, 2004). Overexpression of *GIF1* and of several *GRFs* results in plants with larger organs due to increased cell proliferation (Lee et al., 2009; Vercruysse et al., 2020). *gif1* mutants, on the other hand, show the opposite phenotype, i.e. plants with smaller and narrower leaves as a result of reduced cell number (Kim & Kende, 2004). Overexpression of miR396 leads to post-transcriptional downregulation of *GRFs* containing its target site and to plants with narrow leaves due to cell number reduction (Liu et al., 2009). Conversely, plants transformed with miR396-resistant variants of *GRFs* display a higher cell number and larger leaves (Debernardi et al., 2014; Rodriguez et al., 2010).

When *NAT2*$_{UGT73C6}$ is overexpressed, we detected a significant increase in the levels of *GRF6*, *GRF4* and *GRF9* transcripts, which is more pronounced for the latter two in the tip region of the leaf (Figure 6d). We observed an increase in *GRF6* levels in the bottom part of the leaf of the *NAT2*$_{UGT73C6}$ overexpressing line while they were reduced in the line where *NATs*$_{UGT73C6}$ were downregulated (Figure 6e), suggesting that the presence of the *NATs*$_{UGT73C6}$ is important for maintaining wild-type *GRF6* mRNA levels. Interestingly, *GRF6*, like *GRF5*, lacks the miR396 binding site. Despite this fact, *GRF6* expression is reduced in plants overexpressing the miRNA suggesting a feed-forward effect of the other *GRFs* on its levels (Rodriguez et al., 2010). In addition, *GIF1* expression was also found to be significantly increased in both leaf regions of the *NAT2*$_{UGT73C6}$ overexpressing line (Figure 6d).

The GRF-GIF duo is known to activate their own transcription through a positive feedback regulatory loop (Vercruyssen et al., 2014). Accordingly, increases in GRFs due to a higher transcript abundance could lead to an increment of *GIF1* transcripts in the *NAT2*$_{UGT73C6}$ overexpression line. Simultaneous expression of high levels of *GRF3* and *GIF1* transcripts results in a synergistic increase in leaf cell number and additive effects on gene expression (Debernardi et al., 2014), suggesting that the phenotype in the overexpression lines may be enhanced by the concurrent increased levels of *GRFs* and *GIF1*.

We observed an increase in rosette area exclusively when we overexpressed the full-length *NATs*$_{UGT73C6}$ molecules (Figures 4 and 5b). Based on this observation and on the fact that both *NATs*$_{UGT73C6}$ differ in the 5′-region, it is conceivable that the function(s) of the *NATs*$_{UGT73C6}$ are only enabled by a complex structure formed by the full-length RNAs containing the complete 3′-region. Such a situation has been described for *HIDDEN TREASURE 1* (*HID1*;

© 2022 The Authors.

1365313x, 2023, 3, Downloaded from https://onlinelibrary.wiley.com/doi/10.1111/tpj.16058 by Universite Paris-Saclay, Wiley Online Library on [05/04/2023]. See the Terms and Conditions (https://onlinelibrary.wiley.com/terms-and-conditions) on Wiley Online Library for rules of use; OA articles are governed by the applicable Creative Commons License

Wang et al., 2014), a lncRNA containing four main stem-loops of which two are essential for its function, the regulation of *PHYTOCHROME-INTERACTING FACTOR 3* (*PIF3*) gene expression. On the other hand, these data may be indicative of interaction with RNA-binding proteins that may be required for the functionality of the lncNATs and that bind exclusively to full-length $NATs_{UGT73C6}$ molecules.

TWISTED LEAF (*TL*), an endogenous lncRNA from rice, was previously reported to influence leaf blade shape by modulating the expression of the gene encoding the *R2R3 MYB* transcription factor with which it overlaps (Liu et al., 2018). However, to our knowledge, our work represents the first report of lncNATs involved in leaf size regulation. Although the presence of a potential miRNA396 binding site suggests a target mimicking activity of $NATs_{UGT73C6}$, our preliminary *in vitro* experiments (data not shown) do not support this idea and indicate that other mechanism(s) must be responsible for the detected changes in *GRFs* and *GIF1* expression.

EXPERIMENTAL PROCEDURES

Plant material and growth conditions

Arabidopsis thaliana ecotype Columbia 0 (Col-0) was used as wild-type. All generated transgenic lines and the *ugt73c6ko* knockout mutant (SAIL_525_H07; Jones et al., 2003) were on the same Col-0 genetic background. Seeds were surface sterilized, stratified for 3 days at 4°C and sown on 0.5 × solid Murashige and Skoog (MS) medium supplemented with 1% (w/v) sucrose. Seedlings were grown in a growth chamber under LDs (16 h light/ 8 h dark) at 22°C/20°C. To evaluate phenotypes in adult plants, 10-day-old seedlings were transferred to individual pots filled with steam-sterilized soil and maintained in the greenhouse or in growth chambers (Percival Scientific, Perry, IA, USA) under LDs and controlled temperature (22°C/20°C) and humidity (65–70%).

Generation of transgenic lines

For the generation of $NAT1_{UGT73C6}$ and $NAT2_{UGT73C6}$ overexpressing plants, the sequences reported in the TAIR10 database were PCR amplified from genomic DNA extracted from *A. thaliana* plants. The same template was used for the amplification of the promoter regions of $NAT1_{UGT73C6}$ and $NAT2_{UGT73C6}$ (2045 and 2580 bp starting immediately upstream of the respective reported TIS), and of the promoters of *UGT73C6* (bases −1687 to +4 considering the translation initiation site) and *UGT73C5* (759 bp upstream of the translation initiation site). The amplicons, starting with a non-template CACC sequence, were directionally cloned into the pENTR™/D-TOPO vector (Life Technologies, Carlsbad, CA, USA).

The pENTR clone containing the genomic $NAT2_{UGT73C6}$ sequence was further used as template for start codon(s) removal by site-directed mutagenesis in PCR reactions with AccuPrime Pfx DNA polymerase (Thermo Fisher Scientific, Waltham, MA, USA) and overlapping primers in which the ATG codons were replaced by the CCC trinucleotide. The plasmid containing the insert with the desired mutations, introduced by repeated rounds of mutagenesis, was used as donor for gateway cloning.

Sequence identity and absence of unwanted mutations were confirmed by sequencing (Eurofins Genomics, Ebersberg, Germany) of the inserts present in the pENTR clones. The inserts were recombined into the destination vectors using LR clonase™ II Enzyme mix (Invitrogen, Waltham, MA, USA). pB7WG2 and pBGWFS7 vectors (Karimi et al., 2002) were used to generate overexpression and promoter-reporter lines, respectively.

The amiRNA candidates were selected using the P-SAMS amiRNA Designer tool (http://p-sams.carringtonlab.org/; Carbonell et al., 2014), and constructs for plant transformation were generated according to the protocol provided by the authors. Destination vectors pMDC32B-AtMIR390a-B/c and pMDC123SB-AtMIR390a-B/c were used, which allowed plant selection with hygromycin or with the herbicide glufosinate-ammonium (BASTA®, Bayer AG, Leverkusen, Germany), respectively.

The presence and identity of the cloned products in the pDEST vectors was verified by colony PCR and restriction analysis. Binary plasmids were introduced by electroporation into the *Agrobacterium tumefaciens* strain GV3101, and suspensions of the transformed bacteria were used for transformation of *A. thaliana* by the floral-dip method (Clough & Bent, 1998). Transgenic plants were selected based on Mendelian segregation of the resistance gene. Transgene expression levels were determined by Northern blot or qRT-PCR.

RNA extraction and qRT-PCR

Total RNA was extracted from seedlings and rosette leaves using the peqGOLD Plant RNA kit (PeqLab, Erlangen, Germany) according to the manufacturer's instructions. Genomic DNA was removed using double-stranded specific DNase (dsDNase; Thermo Fisher Scientific). First-strand cDNA was synthesized with SuperScript II (Thermo Fisher Scientific) using oligo dT or gene-specific primers. Amplicons were obtained by PCR using Phusion or Dream-Taq (Thermo Fisher Scientific), and expression levels quantified by qRT-PCR with a QuantStudio5 Real-Time instrument (Thermo Fisher Scientific) using FAST SYBR™ Green qPCR Master Mix (Thermo Fisher Scientific). Gene expression was normalized to the reference genes *Protein phosphatase 2A subunit* (*PP2AA3*, *At1g13320*) or *Glyceraldehyde-3-phosphate dehydrogenase C*-2 (*GAPC2*, *At1g13440*; Czechowski et al., 2005). $\Delta\Delta C_t$ values represent the mean difference in ΔC_t between treatment and control samples or between mutants and control plants.

GUS staining

Plant material from homozygous transgenic lines carrying the GUS reporter constructs was first incubated overnight at 37°C in GUS staining solution [0.5 mM $K_4Fe(CN)_6$, 0.5 mM $K_3Fe(CN)_6$, 0.1% Triton X-100, 0.5 mg ml^{-1} X-Gluc in dimethylformamide, 50 mM NaH_2PO_4, pH 7.0]. Chlorophyll was then removed by incubation in aqueous solutions containing increasing concentrations of ethanol [20, 35, 50 and 70% (v/v) final concentration] and samples were stored in 70% (v/v) ethanol. Pictures were taken with a SMZ1270® stereomicroscope (Nikon, Tokyo, Japan).

BR treatment

The experiments were performed as previously reported (Husar et al., 2011). Briefly, Col-0 seedlings were grown vertically in 0.5 × solid MS medium for 5 days, transferred to sterile flasks containing 0.5 × liquid MS medium and incubated, with shaking, for 2 days in continuous light. 24-Epi-brassinolide (epiBL, Sigma Aldrich®, St Louis, MO, USA) dissolved in dimethyl sulfoxide (DMSO) was added to a final concentration of 1 μM, and the seedlings were further incubated under the conditions described. Control seedlings were supplemented with the same volume of DMSO. Samples were collected at different times (0, 10, 30 and

© 2022 The Authors.

1365313x, 2023, 3, Downloaded from https://onlinelibrary.wiley.com/doi/10.1111/tpj.16058 by Universite Paris-Saclay, Wiley Online Library on [05/04/2023]. See the Terms and Conditions (https://onlinelibrary.wiley.com/terms-and-conditions) on Wiley Online Library for rules of use; OA articles are governed by the applicable Creative Commons License

60 min, 2, 3 and 24 h), snap-frozen in liquid nitrogen and stored at −80°C until analysis.

RNA half-life determination

RNA half-lives were determined as previously described (Fedak et al., 2016). Col-0 seedlings were grown vertically for 11 days on 0.5 × MS medium, and then transferred to a six-well plate containing incubation buffer (1 mM PIPES pH 6.25, 1 mM trisodium citrate, 1 mM KCl, 15 mM sucrose). After 30 min incubation, cordycepin (3′ deoxyadenosine) was added to a final concentration of 150 mg L^{-1} and internalized by vacuum (two cycles of 5 min each). Seedlings were collected at regular time points every 15 min (0, 15, 30, 45, 60, 75, 90, 105 and 120 min) and frozen in liquid nitrogen. Gene expression analyzed by qRT-PCR and the short- and long-lived transcripts *EXPANSIN-LIKE1* (*Expansin L1*) and *Eukaryotic translation initiation factor 4A1* (*EIF4A1A*) were used as controls. C_t-values were normalized by the C_t-value at time point 0 [$C_{t(n)} = \ln(C_t/C_{t(0)}) \times (-10)$] and plotted as degradation curves. The slopes of the curves were used to calculate RNA half-live [$t_{1/2} = (\ln 2)/\text{slope}$].

Rosette and leaf area measurements

Complete plant images were taken with a digital camera (Sony® DSLR, Sony, Tokyo, Japan). For determination of the rosette area, digital images of 20–30 plants per line were analyzed with the Easy Leaf Area program (Easlon & Bloom, 2014) and the green area quantified. The area of individual leaves was measured with ImageJ (Schneider et al., 2012).

Microscopic analysis, cell size determination and cell number estimation

Leaf material for microscopic analysis was prepared according to Nelissen et al. (2013) with modifications. Leaf 6 of selected 35-day-old plants were incubated in fixation solution (90% absolute ethanol, 10% acetic acid) for 2 h, followed by overnight incubation in 90% ethanol. Samples were placed in 70% ethanol for 30 min, stored in lactic acid and transferred to Hoyer medium (80 g chloral hydrate in 30 ml water) for clearing prior to microscopic analysis. Leaves were cut into four sections along the longitudinal axis, and mesophyll and abaxial epidermal cells were imaged from the tip and bottom regions by differential interference contrast microscopy using an Apotome.2 microscope (ZEISS, Jena, Germany) and an Axiocam ERc 5s microscope camera (ZEISS). Cell borders were manually drawn on the photo using the Vectornator program (https://www.vectornator.io), or analogously after printing the photos on transparent sheet, scanning and processing them with the Fiji processing package (https://fiji.sc/; Schindelin et al., 2012) to obtain individual cell area. A lower limiting size of 2000 μm^2 was used to quantify only the fully developed palisade mesophyll cells.

The total number of palisade mesophyll and abaxial epidermal cells on leaf 6 was estimated by dividing the determined area of individual leaves by the mean cell area of each cell type. For epidermal cells, an upper limit of 15 000 μm^2 was set to exclude abnormally large cells (less than 4% for all lines except for *OE-*$NAT2_{UGT73C6}$*-6*, where they represent 5.7%).

In silico and statistical analyses

The potential protein-coding capacity from both $NATs_{UGT73C6}$ was determined with the ExPASy translation tool (https://web.expasy.org/translate/), and protein domains were analyzed with the Pfam database web tool (www.pfam.xfam.org) and PROSITE (www.prosite.expasy.org).

Data were tested with unpaired two-tailed Student's *t*-test or one-way analysis of variance and Tukey's honestly significance test using GraphPad Prism 7 software (GraphPad Software, San Diego, CA, USA). Graphs were generated with the same software.

Primers

All primers used in this study are listed in Data S2.

AUTHOR CONTRIBUTIONS

SG-Z designed the experiments and wrote the manuscript. SKM, MH, SE, AJ, TdV, ST, KB-K and SG-Z generated the constructs and the transgenic lines, performed the experiments, and analyzed the results. MH, SKM, SE and SG-Z produced the figures. SA and S-EB contributed with conceptual input and comments. All authors read and approved the final article.

ACKNOWLEDGEMENTS

The authors thank Alberto Carbonell (IBMCP, Spain) for the design of the amiGUS constructs, James Carrington (Donald Danforth Plant Science Center, USA) for providing vectors for the expression of amiRNAs, Brigitte Poppenberger (TUM, Germany) for seeds of the *OE-UGT73C5* line, and Silvestre Marillonet (IPB, Germany) for providing the p19 clone. The authors thank Gary Sawers (MLU, Germany) for reading the manuscript, and Sabine Rosahl (IPB, Germany) for conceptual input and comments. The authors thank Kristin Eismann and Michael André Fritz for technical assistance and initial data, respectively. This work was supported by grants from the Deutsche Forschungsgemeinschaft (DFG) [RTG1591 (projects C2 to S.E.B. and C3 to S.G.-Z.)], the European Union [ERASMUS MUNDUS Action 2 program 'BRAVE'], the State Research Priority Program Saxony-Anhalt Fkz [ZS/2016/06/79740] (to S.G.-Z. and S.E.B.), and the core funding of the state of Saxony-Anhalt and the Federal Republic of Germany to IPB. S.K.M. was funded by a BRAVE scholarship, by IPB and by RTG1591 projects C2 and C3. S.E. was funded by RTG1591 project C2 and by IPB. A.J. was funded by RTG1591 project C3. S.G.Z. was funded by the Priority Program and IPB. Open Access funding enabled and organized by Projekt DEAL.

CONFLICT OF INTEREST

The authors declare that they have no conflicts of interest for this work.

DATA AVAILABILITY STATEMENT

All relevant data can be found within the manuscript and its supporting materials.

SUPPORTING INFORMATION

Additional Supporting Information may be found in the online version of this article.

Figure S1. Histochemical localization of GUS activity at different developmental stages in the Pro$NAT1_{UGT73C6}$*:GUS* and Pro$NAT2_{UGT73C6}$*:GUS* transgenic lines.

Figure S2. $NATs_{UGT73C6}$ and *UGT73C6* expression levels reported in the Arabidopsis RNA-Seq Database (ARS).

© 2022 The Authors.

1365313x, 2023, 3, Downloaded from https://onlinelibrary.wiley.com/doi/10.1111/tpj.16058 by Universite Paris-Saclay, Wiley Online Library on [05/04/2023]. See the Terms and Conditions (https://onlinelibrary.wiley.com/terms-and-conditions) on Wiley Online Library for rules of use; OA articles are governed by the applicable Creative Commons License

Figure S3. Determination of $NATs_{UGT73C6}$ and *UGT73C6* ends by 5′ circular RACE and conventional 3′ RACE.

Figure S4. Identification of $NAT2_{UGT73C6}$ splice variants.

Figure S5. Gene expression analysis and rosette area quantification in the $ugt73c6_{ko}$ line.

Figure S6. Identification and characterization of transgenic lines with reduced $NATs_{UGT73C6}$ expression.

Figure S7. Expression analysis in transgenic lines transformed with the $NATs_{UGT73C6}$ sequences and leaf growth kinematics.

Figure S8. Detection of small peptides encoded by $NAT2_{UGT73C6}$ via transient expression assays in *Nicotiana benthamiana*.

Figure S9. Transcript levels of $NATs_{UGT73C6}$ in transgenic lines transformed with $NAT2_{UGT73C6}$ or its mutant variant $_{mut}NAT2_{UGT73C6}$.

Figure S10. *UGT73C5* transcript levels in lines with altered $NATs_{UGT73C6}$ expression.

Figure S11. Early response to brassinosteroid treatment and expression of brassinosteroid marker genes.

Figure S12. Histochemical localization of GUS activity in a young leaf of the Pro$NAT2_{UGT73C6}$:*GUS* transgenic line and potential miRNA396 binding site in the $NATs_{UGT73C6}$ sequence.

Table S1. Statistical indices of the growth curves of leaves 1–6 of the $NATs_{UGT73C6}$ knockdown line ($_{amiR}NATs_{UGT73C6}$-*10*) and the control.

Table S2. Statistical indices of the growth curves of leaves 1–6 of the line with increased $NAT2_{UGT73C6}$ expression (*OE-*$NAT2_{UGT73C6}$-*6*) and the control.

Data S1. Experimental procedures and results of transient expression assays in *Nicotiana benthamiana*.

Data S2. Oligonucleotides used in this study.

REFERENCES

Andriankaja, M., Dhondt, S., De Bodt, S., Vanhaeren, H., Coppens, F., De Milde, L. *et al.* (2012) Exit from proliferation during leaf development in *Arabidopsis thaliana*: a not-so-gradual process. *Developmental Cell*, **22**, 64–78.

Ariel, F., Romero-Barrios, N., Jegu, T., Benhamed, M. & Crespi, M. (2015) Battles and hijacks: noncoding transcription in plants. *Trends in Plant Science*, **20**, 362–371.

Ben Amor, B., Wirth, S., Merchan, F., Laporte, P., D'Aubenton-Carafa, Y., Hirsch, J. *et al.* (2009) Novel long non-protein coding RNAs involved in Arabidopsis differentiation and stress responses. *Genome Research*, **19**, 57–69.

Borsani, O., Zhu, J., Verslues, P.E., Sunkar, R. & Zhu, J.K. (2005) Endogenous siRNAs derived from a pair of natural cis-antisense transcripts regulate salt tolerance in Arabidopsis. *Cell*, **123**, 1279–1291.

Caputi, L., Malnoy, M., Goremykin, V., Nikiforova, S. & Martens, S. (2012) A genome-wide phylogenetic reconstruction of family 1 UDP-glycosyltransferases revealed the expansion of the family during the adaptation of plants to life on land. *The Plant Journal*, **69**, 1030–1042.

Carbonell, A., Takeda, A., Fahlgren, N., Johnson, S.C., Cuperus, J.T. & Carrington, J.C. (2014) New generation of artificial microRNA and synthetic trans-acting small interfering RNA vectors for efficient gene silencing in Arabidopsis. *Plant Physiology*, **165**, 15–29.

Chen, L.L. (2016) Linking long noncoding RNA localization and function. *Trends in Biochemical Sciences*, **41**, 761–772.

Clark, M.B., Johnston, R.L., Inostroza-Ponta, M., Fox, A.H., Fortini, E., Moscato, P. *et al.* (2012) Genome-wide analysis of long noncoding RNA stability. *Genome Research*, **22**, 885–898.

Clough, S.J. & Bent, A.F. (1998) Floral dip: a simplified method for agrobacterium-mediated transformation of *Arabidopsis thaliana*. *The Plant Journal*, **16**, 735–743.

Csorba, T., Questa, J.I., Sun, Q. & Dean, C. (2014) Antisense COOLAIR mediates the coordinated switching of chromatin states at FLC during vernalization. *Proceedings of the National Academy of Sciences of the United States of America*, **111**, 16160–16165.

Cui, J., Luan, Y., Jiang, N., Bao, H. & Meng, J. (2017) Comparative transcriptome analysis between resistant and susceptible tomato allows the identification of lncRNA16397 conferring resistance to *Phytophthora infestans* by co-expressing glutaredoxin. *The Plant Journal*, **89**, 577–589.

Czechowski, T., Stitt, M., Altmann, T., Udvardi, M.K. & Scheible, W.R. (2005) Genome-wide identification and testing of superior reference genes for transcript normalization in Arabidopsis. *Plant Physiology*, **139**, 5–17.

Debernardi, J.M., Mecchia, M.A., Vercruyssen, L., Smaczniak, C., Kaufmann, K., Inze, D. *et al.* (2014) Post-transcriptional control of GRF transcription factors by microRNA miR396 and GIF co-activator affects leaf size and longevity. *The Plant Journal*, **79**, 413–426.

Deforges, J., Reis, R.S., Jacquet, P., Sheppard, S., Gadekar, V.P., Hart-Smith, G. *et al.* (2019) Control of cognate sense mRNA translation by cis-natural antisense RNAs. *Plant Physiology*, **180**, 305–322.

Easlon, H.M. & Bloom, A.J. (2014) Easy leaf area: automated digital image analysis for rapid and accurate measurement of leaf area. *Applied Plant Science*, **2**, apps.1400033.

Fedak, H., Palusinska, M., Krzyczmonik, K., Brzezniak, L., Yatusevich, R., Pietras, Z. *et al.* (2016) Control of seed dormancy in Arabidopsis by a cis-acting noncoding antisense transcript. *Proceedings of the National Academy of Sciences of the United States of America*, **113**, E7846–E7855.

Goda, H., Shimada, Y., Asami, T., Fujioka, S. & Yoshida, S. (2002) Microarray analysis of brassinosteroid-regulated genes in Arabidopsis. *Plant Physiology*, **130**, 1319–1334.

Gonzalez, N., Vanhaeren, H. & Inze, D. (2012) Leaf size control: complex coordination of cell division and expansion. *Trends in Plant Science*, **17**, 332–340.

Henriques, R., Wang, H., Liu, J., Boix, M., Huang, L.F. & Chua, N.H. (2017) The antiphasic regulatory module comprising CDF5 and its antisense RNA FLORE links the circadian clock to photoperiodic flowering. *The New Phytologist*, **216**, 854–867.

Husar, S., Berthiller, F., Fujioka, S., Rozhon, W., Khan, M., Kalaivanan, F. *et al.* (2011) Overexpression of the UGT73C6 alters brassinosteroid glucoside formation in *Arabidopsis thaliana*. *BMC Plant Biology*, **11**, 51.

Jabnoune, M., Secco, D., Lecampion, C., Robaglia, C., Shu, Q. & Poirier, Y. (2013) A rice cis-natural antisense RNA acts as a translational enhancer for its cognate mRNA and contributes to phosphate homeostasis and plant fitness. *Plant Cell*, **25**, 4166–4182.

Jones, P., Messner, B., Nakajima, J., Schaffner, A.R. & Saito, K. (2003) UGT73C6 and UGT78D1, glycosyltransferases involved in flavonol glycoside biosynthesis in *Arabidopsis thaliana*. *The Journal of Biological Chemistry*, **278**, 43910–43918.

Jones-Rhoades, M.W. & Bartel, D.P. (2004) Computational identification of plant microRNAs and their targets, including a stress-induced miRNA. *Molecular Cell*, **14**, 787–799.

Kalve, S., Fotschki, J., Beeckman, T., Vissenberg, K. & Beemster, G.T. (2014) Three-dimensional patterns of cell division and expansion throughout the development of *Arabidopsis thaliana* leaves. *Journal of Experimental Botany*, **65**, 6385–6397.

Karimi, M., Inze, D. & Depicker, A. (2002) GATEWAY vectors for Agrobacterium-mediated plant transformation. *Trends in Plant Science*, **7**, 193–195.

Kim, J.H. & Kende, H. (2004) A transcriptional coactivator, AtGIF1, is involved in regulating leaf growth and morphology in Arabidopsis. *Proceedings of the National Academy of Sciences of the United States of America*, **101**, 13374–13379.

Kindgren, P., Ard, R., Ivanov, M. & Marquardt, S. (2018) Transcriptional read-through of the long non-coding RNA SVALKA governs plant cold acclimation. *Nature Communications*, **9**, 4561.

Lapidot, M. & Pilpel, Y. (2006) Genome-wide natural antisense transcription: coupling its regulation to its different regulatory mechanisms. *EMBO Reports*, **7**, 1216–1222.

Lee, B.H., Ko, J.H., Lee, S., Lee, Y., Pak, J.H. & Kim, J.H. (2009) The Arabidopsis GRF-INTERACTING FACTOR gene family performs an overlapping function in determining organ size as well as multiple developmental properties. *Plant Physiology*, **151**, 655–668.

Lin, S., Zhang, L., Luo, W. & Zhang, X. (2015) Characteristics of antisense transcript promoters and the regulation of their activity. *International Journal of Molecular Sciences*, **17**, 9.

© 2022 The Authors.

1365313x, 2023, 3, Downloaded from https://onlinelibrary.wiley.com/doi/10.1111/tpj.16058 by Universite Paris-Saclay, Wiley Online Library on [05/04/2023]. See the Terms and Conditions (https://onlinelibrary.wiley.com/terms-and-conditions) on Wiley Online Library for rules of use; OA articles are governed by the applicable Creative Commons License

Liu, D., Song, Y., Chen, Z. & Yu, D. (2009) Ectopic expression of miR396 suppresses GRF target gene expression and alters leaf growth in Arabidopsis. *Physiologia Plantarum*, **136**, 223–236.

Liu, X., Li, D., Zhang, D., Yin, D., Zhao, Y., Ji, C. *et al.* (2018) A novel antisense long noncoding RNA, TWISTED LEAF, maintains LEAF blade flattening by regulating its associated sense R2R3-MYB gene in rice. *The New Phytologist*, **218**, 774–788.

Mercer, T.R., Dinger, M.E. & Mattick, J.S. (2009) Long non-coding RNAs: insights into functions. *Nature Reviews. Genetics*, **10**, 155–159.

Nelissen, H., Rymen, B., Coppens, F., Dhondt, S., Fiorani, F. & Beemster, G.T. (2013) Kinematic analysis of cell division in leaves of mono- and dicotyledonous species: a basis for understanding growth and developing refined molecular sampling strategies. *Methods in Molecular Biology*, **959**, 247–264.

Poppenberger, B., Fujioka, S., Soeno, K., George, G.L., Vaistij, F.E., Hiranuma, S. *et al.* (2005) The UGT73C5 of *Arabidopsis thaliana* glucosylates brassinosteroids. *Proceedings of the National Academy of Sciences of the United States of America*, **102**, 15253–15258.

Reis, R.S. & Poirier, Y. (2021) Making sense of the natural antisense transcript puzzle. *Trends in Plant Science*, **26**, 1104–1115.

Rinn, J.L. & Chang, H.Y. (2012) Genome regulation by long noncoding RNAs. *Annual Review of Biochemistry*, **81**, 145–166.

Rodriguez, R.E., Mecchia, M.A., Debernardi, J.M., Schommer, C., Weigel, D. & Palatnik, J.F. (2010) Control of cell proliferation in *Arabidopsis thaliana* by microRNA miR396. *Development*, **137**, 103–112.

Rosa, S., Duncan, S. & Dean, C. (2016) Mutually exclusive sense-antisense transcription at FLC facilitates environmentally induced gene repression. *Nature Communications*, **7**, 13031.

Ross, J., Li, Y., Lim, E. & Bowles, D.J. (2001) Higher plant glycosyltransferases. *Genome Biology*, **2**, REVIEWS3004.

Schindelin, J., Arganda-Carreras, I., Frise, E., Kaynig, V., Longair, M., Pietzsch, T. *et al.* (2012) Fiji: an open-source platform for biological-image analysis. *Nature Methods*, **9**, 676–682.

Schneider, C.A., Rasband, W.S. & Eliceiri, K.W. (2012) NIH image to ImageJ: 25 years of image analysis. *Nature Methods*, **9**, 671–675.

Vercruysse, J., Baekelandt, A., Gonzalez, N. & Inze, D. (2020) Molecular networks regulating cell division during Arabidopsis leaf growth. *Journal of Experimental Botany*, **71**, 2365–2378.

Vercruyssen, L., Verkest, A., Gonzalez, N., Heyndrickx, K.S., Eeckhout, D., Han, S.K. *et al.* (2014) ANGUSTIFOLIA3 binds to SWI/SNF chromatin remodeling complexes to regulate transcription during Arabidopsis leaf development. *Plant Cell*, **26**, 210–229.

Wang, H., Chua, N.H. & Wang, X.J. (2006) Prediction of trans-antisense transcripts in Arabidopsis thaliana. *Genome Biology*, **7**, R92.

Wang, H.V. & Chekanova, J.A. (2017) Long noncoding RNAs in plants. *Advances in Experimental Medicine and Biology*, **1008**, 133–154.

Wang, Y., Fan, X., Lin, F., He, G., Terzaghi, W., Zhu, D. *et al.* (2014) Arabidopsis noncoding RNA mediates control of photomorphogenesis by red light. *Proceedings of the National Academy of Sciences of the United States of America*, **111**, 10359–10364.

Wu, L., Liu, S., Qi, H., Cai, H. & Xu, M. (2020) Research progress on plant long non-coding RNA. *Plants (Basel)*, **9**, 408.

Wunderlich, M., Gross-Hardt, R. & Schoffl, F. (2014) Heat shock factor HSFB2a involved in gametophyte development of Arabidopsis thaliana and its expression is controlled by a heat-inducible long non-coding antisense RNA. *Plant Molecular Biology*, **85**, 541–550.

Yu, Y., Zhang, Y., Chen, X. & Chen, Y. (2019) Plant noncoding RNAs: hidden players in development and stress responses. *Annual Review of Cell and Developmental Biology*, **35**, 407–431.

Zhang, X., Lii, Y., Wu, Z., Polishko, A., Zhang, H., Chinnusamy, V. *et al.* (2013) Mechanisms of small RNA generation from cis-NATs in response to environmental and developmental cues. *Molecular Plant*, **6**, 704–715.

Zhao, X., Li, J., Lian, B., Gu, H., Li, Y. & Qi, Y. (2018) Global identification of Arabidopsis lncRNAs reveals the regulation of MAF4 by a natural antisense RNA. *Nature Communications*, **9**, 5056.

© 2022 The Authors.

1365313x, 2023, 3, Downloaded from https://onlinelibrary.wiley.com/doi/10.1111/tpj.16058 by Universite Paris-Saclay, Wiley Online Library on [05/04/2023]. See the Terms and Conditions (https://onlinelibrary.wiley.com/terms-and-conditions) on Wiley Online Library for rules of use; OA articles are governed by the applicable Creative Commons License